

## SOURCE SPECTRA FOR THE 1988 SAGUENAY, QUEBEC, EARTHQUAKES

BY DAVID M. BOORE AND GAIL M. ATKINSON

### ABSTRACT

Source spectra are obtained for the 1988 Saguenay, Quebec, earthquake ( $m_N = 6.5$ ), its foreshock ( $m_N = 4.8$ ), and largest aftershock ( $m_N = 4.1$ ), using recordings from analog and digital seismographs on rock sites at epicentral distances from 40 to 700 km. The source spectra of the foreshock and the aftershock are well matched by a single-corner-frequency  $\omega^{-2}$  model, with seismic moments of  $2.2 \times 10^{22}$  and  $2.2 \times 10^{21}$  dyne-cm, respectively, and a stress parameter of 65 bars for both events. By contrast, the spectrum of the mainshock differs dramatically from this simple shape. A stress parameter of 500 bars is required to match the observed high-frequency amplitudes, using the seismic moment determined from teleseismic observations as a constraint. This single-corner-frequency model, however, overestimates amplitudes at frequencies near 1 Hz by a factor of about 2. The relative radiation of short- and long-period energy for the mainshock is inconsistent with that from other intraplate earthquakes; the fore- and aftershocks appear typical in this regard.

The extraction of source spectra from the regional data required a careful examination of attenuation. Azimuthal variations were observed, with the attenuation being most severe to the southeast (normal to the St. Lawrence Valley and the dominant structural grain of the region). The St. Lawrence River coincides in part with the boundary between the Grenville and Appalachian tectonic provinces, and the difference in attenuation may be related to the difference in tectonic province. The distribution of data, however, makes it difficult to obtain good estimates of the attenuation in each province. Lumping the data from both provinces and the three earthquakes together results in an anelastic attenuation factor given by  $Q = 755f^{0.5}$  for frequencies,  $f$ , from 0.6 to 18 Hz, using data at distances,  $R$ , beyond 100 km from the sources and assuming  $1/\sqrt{R}$  geometrical spreading. This attenuation is similar to that obtained in a number of other studies in the general area. Three-component recordings were available at a few stations, and from these the following frequency-dependent ratio of horizontal-to-vertical motion was obtained:  $H/V = 1.14 + 0.118f - 0.00638f^2$ , for frequencies from 0.2 to 15 Hz.

Different methods of correcting observations for attenuation, in order to derive source spectra, were examined. Source spectra derived by simple regression analyses of observed data, assuming a uniform medium, are very similar to those based on a more complicated synthetic seismogram correction, which accounts for wave propagation in a layered Earth.

### INTRODUCTION

Predictions of ground motion in eastern North America are hindered by a lack of data for the large events of most engineering interest. For this reason, the occurrence of the Saguenay, Quebec, earthquake on 25 November 1988 is of exceptional interest. With a short-period magnitude ( $m_N$ ) of 6.5, this is the largest earthquake to have occurred in eastern North America within the last 50 years. The earthquake is an enigma in several respects: it was deeper than most events (28 km rather than 5 to 15), it occurred in a region essentially devoid of seismicity (North *et al.*, 1989), and the high-frequency spectral level of

the radiation at the source was surprisingly large. The mainshock was preceded by a foreshock with  $m_N = 4.8$ . There were only a few significant aftershocks, the largest of which had a magnitude of  $m_N = 4.1$ . These events were also deep (25 to 30 km) but, in contrast to the mainshock, their radiation was not particularly rich in high-frequency energy. (Information about the events is summarized in Table 1; the terms "foreshock" and "aftershock" will refer to the events in the table.)

The earthquakes were well recorded on a variety of instruments. The mainshock was recorded on a network of three-component, film-recording strong-motion accelerographs (hereafter referred to as the SMA network) at distances of 40 to 150 km (Munro and Weichert, 1989). Regional seismographic stations of the digital Eastern Canada Telemetered Network (ECTN) recorded the foreshock and aftershocks in addition to the mainshock, although the  $Lg$  phase of the mainshock was clipped at the closest stations. The mainshock was also recorded at about a dozen digital accelerograph stations in the northeastern United States (NCEER network) (Friberg *et al.*, 1988). The locations of recording stations with respect to the focus of the earthquakes (the events are approximately co-located) are shown on Figure 1. The mainshock was recorded at teleseismic distances and on a broadband instrument at Harvard (Zhao and Helmberger, 1992).

The Saguenay mainshock has been studied by several authors: Boatwright and Choy (1992) derived the source spectra up to a frequency of 2 Hz from teleseismic  $P$  waves; Somerville *et al.* (1990) modeled the event using a combination of teleseismic and strong-motion data; and both Gariel and Jacob (1989) and Ou and Herrmann (1990) fit models to the peak acceleration data. The Boatwright and Choy and the Somerville *et al.* studies find that the event is not well described by a simple  $\omega^{-2}$  source model, and the results of all the studies are consistent with the conclusion that the mainshock was particularly energetic at high frequencies. The anomalous high-frequency energy manifests itself in different ways for each of these studies: to model the observed high-frequency amplitudes, Gariel and Jacob use a moment almost 10 times larger than the moment derived from long-period data at teleseismic distances; Ou and Herrmann use the observed moment, with a high stress parameter (320 bars); Somerville *et al.*'s model uses the observed moment with an overall stress drop of 160 bars, but they base their source-time function on the recording at SMA station S17, thus guaranteeing the enrichment of high-frequency motions neces-

TABLE 1  
SAGUENAY EARTHQUAKES: LOCATIONS AND MAGNITUDES

Event	MM/DD/YY	HH:MM:SS	Latitude ( $^{\circ}$ N)	Longitude ( $^{\circ}$ W)	Depth (km)	$m_N$	M
FS	11/23/88	09:11:27	48.13	71.20	28	4.8	4.2
MS	11/25/88	03:46:04	48.12	71.18	29	6.5	5.8
AS	11/26/88	03:38:08	48.14	71.30	30	4.1	3.5

Epicenter information from Geological Survey of Canada (R. Wetmiller, oral comm., 1989, 1991). Depths of 26 km for the MS and 25 km for the AS have been reported by Somerville *et al.* (1990) and North *et al.* (1989), respectively.

$m_N$  (Nuttli magnitude; also known as  $m_{bLg}$ ) from North *et al.* (1989).

M (moment magnitude) for the FS and AS from the determinations of seismic moment in this paper and for the MS from G. Ekström (personal comm. to J. Boatwright, 1991).

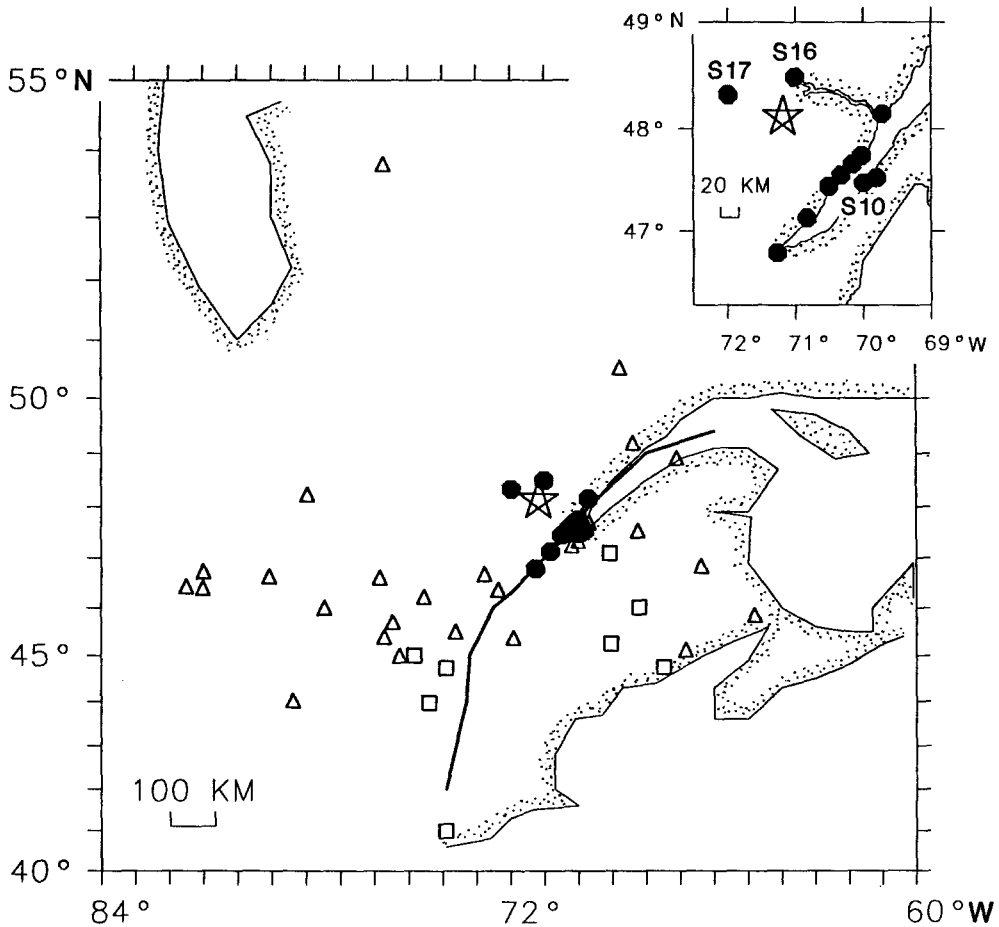


FIG. 1. Map showing epicenter of mainshock (star) and locations of the strong-motion analog recorders (filled circles), ECTIN stations (triangles), and NCEER stations (squares). The landward edge of the shoreline is stippled. While the locations of the stations are accurately plotted, the shoreline has been depicted crudely (except on the inset); it only serves as a rough reference to geographic features. The heavy line represents the boundary between the Grenville tectonic province (to the left) and the Appalachian tectonic province (to the right). The aftershock and foreshock locations were located within 10 km of the mainshock and have not been plotted in this figure.

sary to fit the peak accelerations and peak velocities. The enrichment of high-frequency motions is also supported by the simple observation that the short-period magnitude,  $m_N = 6.5$ , is unusually large relative to the moment magnitude,  $M = 5.8$ .

The complicated shape and the enhanced high-frequency radiation of the mainshock are not reflected in the simple source model assumed in the derivation of theoretical ground motion relations for eastern North America (Boore and Atkinson, 1987; Toro and McGuire, 1987; Atkinson and Boore, 1990). For this reason, the ground motions from the Saguenay earthquake were substantially larger at high frequencies than predicted by the published relations, as shown in Figure 2.

Our primary goal in this study is to obtain the source spectra of the largest Saguenay earthquakes. To do this, we use the  $S$  and  $Lg$  phases on all available

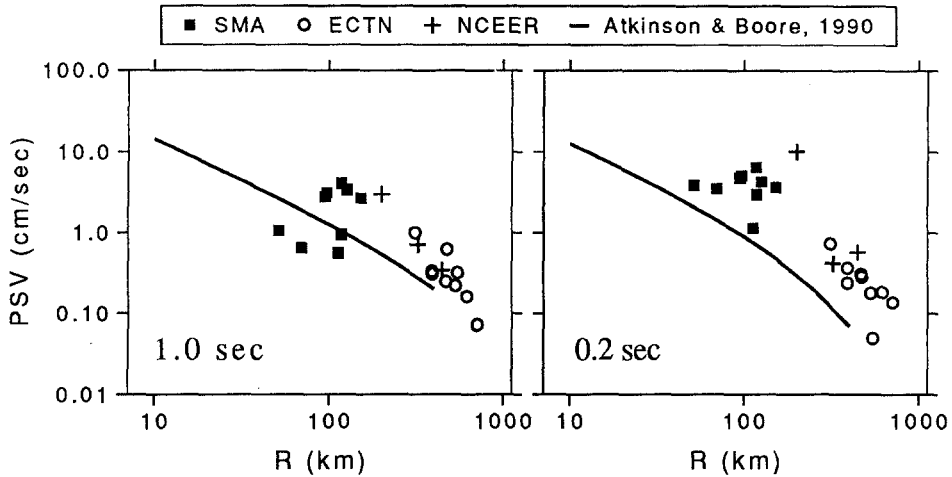


FIG. 2. Pseudo-relative velocity spectra ( $PSV$ ) for 5%-damped oscillators with periods of 1.0 and 0.2 sec. The symbols are values computed from data recorded on the indicated networks, and the solid line is the prediction using the equations in Atkinson and Boore (1990), using  $M = 5.8$ . The abscissa is hypocentral distance. The SMA and NCEER points are the average of the logarithms of the  $PSV$  from the two horizontal components; the ECTN values are from vertical components (horizontal components are not available), corrected for the difference between horizontal and vertical components by adding 0.12 and 0.20 to the  $\log PSV$  values, for the 1.0- and 0.2-sec oscillators, respectively. These correction factors were guided by the results in the text and by the  $\log H/V$  values computed from the SMA and NCEER data (0.08 and 0.17 for 1 sec and 0.08 and 0.34 for 0.2 sec). Data from more NCEER stations are available at greater distances, but these data exhibit obvious quantization steps and have been excluded for that reason (see Atkinson, 1991, for an example).

components of the SMA and ECTN stations to derive source spectra for the foreshock, mainshock, and aftershock for frequencies from about 0.5 to 20 Hz. The source spectra are obtained for a higher-frequency range than that covered by previous studies of the mainshock, largely because we use different data and analysis methods. The source spectra for the fore- and aftershocks have not been previously studied. We first derive the source spectrum of the mainshock from the closest recording, using a simple model to correct for wave propagation effects. We then present both the frequency-dependent attenuation measured for the dominant energy beyond 100 km and the ratio of horizontal to vertical motion. This information is used to derive the source spectra for the three events, using data recorded at many distances and azimuths. Three different schemes for relating the observed spectra to the source spectra are employed, two of which use synthetic seismogram calculations to correct for the source excitation and wave propagation in a layered Earth. Finally, we discuss in an appendix some intriguing differences in high-frequency spectral decay of records from the SMA stations.

#### INITIAL ANALYSIS OF THE MAINSHOCK FROM SMA DATA

To obtain an initial estimate of the source spectrum of the mainshock, we use the data collected at station S16. At an epicentral distance of 43 km, this is the SMA station closest to the source. The advantage of using this station is that path effects should be minimized; as demonstrated by the synthetic seismograms of Somerville *et al.* (1990), the direct  $S$  waves should dominate the record. (As we note in Appendix A, however, the energy in the record is

drawn out over a much longer time than predicted by the synthetic seismograms; this is presumably due to strong scattering in the region. Fig. A2, however, shows that the spectra are not particularly sensitive to the presence of the coda). Another advantage to using S16 is that our calculations of the radiation patterns for a collection of published focal mechanisms (summarized in Haddon, 1992) show that neither the direct *SV* nor the direct *SH* waves are near nodes.

The source spectrum of the mainshock was estimated from the two horizontal components of the *S* wave recorded at S16, using the following relation between the source spectrum ( $S_a(f)$ ) and the observed acceleration spectrum ( $A_{obs}(f)$ ) (e.g., Boore and Atkinson, 1987):

$$S_a(f) = [4\pi\rho_0\beta_0^3R] \left[ \exp\left(\frac{\pi fR}{Q\beta_0}\right) \right] A_{obs}, \quad (1)$$

where  $\rho_0$  and  $\beta_0$  are density and shear velocity near the source,  $R$  is the hypocentral distance, and the frequency-dependent attenuation parameter  $Q$  is determined by the regression analysis of the data, as discussed later (at the short distance to station S16 the  $Q$  correction is relatively unimportant; it corresponds to a factor of about 1.3 at 30 Hz). Equation (1) was derived with the assumption that the product of the free-surface factor, the radiation pattern, and the factor partitioning the motion into the horizontal components is unity. Synthetic seismogram calculations, discussed later, give support to this simple connection between the observed and the source spectra, at least for station S16. The source spectra estimated from the two horizontal components at S16 are shown in Figure 3.

Theoretical source spectra are compared with the estimated source spectrum in Figure 3. The curves show the theoretical spectra for the constant-stress parameter, single-corner-frequency Brune (1970) model for a suite of stress parameters (the equations used for the theoretical curves are given in Appendix B). The assumed moment for the comparisons is  $6.3 \times 10^{24}$  dyne-cm (G. Ekström, personal comm., 1990, based on broadband teleseismic data). (Other values for the mainshock include  $5 \times 10^{24}$  (Somerville *et al.*, 1990),  $8 \times 10^{24}$  (North *et al.*, 1989), and  $8.9 \times 10^{24}$  (Boatwright and Choy, 1992).) The values for the material properties  $\rho_0$  and  $\beta_0$  were taken from Somerville *et al.*'s (1990) velocity model for the region.

#### *Comments on Spectral Shape and Amplitude*

The comparison in Figure 3 contains the essence of our conclusions regarding the mainshock source spectrum, which are merely reinforced by the more detailed analyses presented subsequently. The figure shows that the source is deficient in spectral amplitude around 1 Hz and is enriched in amplitude at higher frequencies. In particular, a stress parameter in excess of 200 bars is needed to explain the spectral level at high frequencies, but a simple  $\omega^{-2}$  model with this stress parameter and the teleseismic moment would greatly overpredict amplitudes at lower frequencies. The S16 spectrum could be fit by an  $\omega^{-2}$  model (note that the spectra are level at high frequencies, as expected for the commonly-used  $\omega^{-2}$  source model), but the required  $M_0$  is much lower than the value obtained from the longer-period teleseismic data, and the required stress

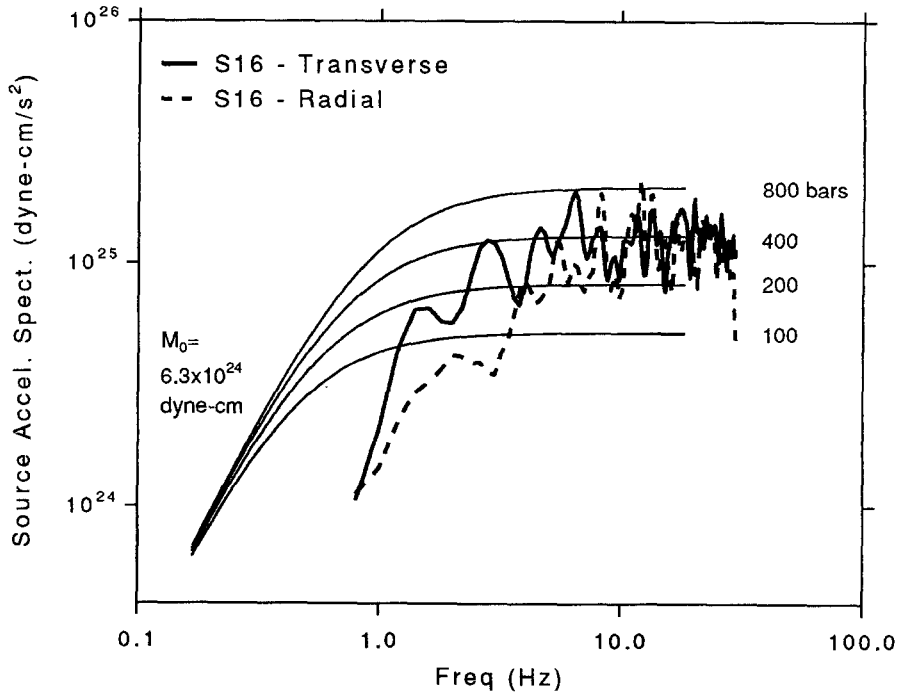


FIG. 3. Source acceleration spectra (as defined in equation B1) computed for the two horizontal components, rotated into transverse and radial directions, of the station (S16) closest to the mainshock (43 km epicentral distance). A low-cut filter at a frequency of 0.67 Hz was employed in the processing of the records (Munro and Weichert, 1989), and therefore the spectra have not been shown below that frequency. The observed acceleration spectra were computed using a 20-sec window; they were smoothed and reduced to source acceleration spectra by using equation (1) with  $\rho_0 = 2.9 \text{ gm/cm}^3$  and  $\beta_0 = 3.7 \text{ km/sec}$ . This is the simplest correction factor, but synthetic calculations using a layered Earth model show that the assumption is adequate for the purposes of this figure. The light lines show theoretical spectra for the indicated moment and stress parameters.

parameter exceeds 1 kbar. We accept the teleseismic estimate of the moment and therefore are led to the conclusion that for the mainshock the source spectrum is not consistent with an  $\omega^{-2}$  model, a finding also reached by Boatwright and Choy (1992). Analysis of data from the next closest station (S17) leads to similar conclusions (see Fig. A1 for a plot of the Fourier spectra from S17).

#### *The Case of the Missing Moment*

The low amplitudes around 1 Hz are manifested in the unusually large low-frequency cutoffs used in the processing of the strong-motion records. These cutoff frequencies range from 0.33 to 0.80 Hz; station S16 had a cutoff frequency of 0.67 Hz (Munro and Weichert, 1989). These cutoff frequencies were based on a comparison of the spectrum from the earthquake signal with the spectrum obtained by processing one of the two digitized fixed-traces as if they were accelerograms (subtracting the other fixed trace to remove long-period errors). The large value of the cutoff frequencies used in the high-pass filter precludes an investigation of the behavior of the spectra at low frequencies from the standard processed accelerograms. To further investigate the Case of the Missing Moment, we obtained the raw digitized data (for all the SMA data) and did

our own processing. Unfortunately, the results are equivocal. Although there is no question that the spectral amplitudes are low around 1 Hz, the spectra of the unfiltered data generally flatten toward lower frequencies and approach the levels expected from the seismic moment (a flattening of a spectrum does not by itself imply the existence of a noise floor). They also approach (but are usually somewhat above) the noise estimates obtained from the fixed-trace analysis. In general, we support the cutoff frequencies used by Munro and Weichert (1989), but there is the possibility that useful signal is present at lower frequencies. As this portion of the spectrum is less important to us than the higher-frequency portion, we have not pursued the matter further.

Because of the possibility of azimuthally dependent source and propagation effects, we are reluctant to base our conclusions about the source spectrum of the mainshock on just the few closest stations. Fortunately, by combining the SMA and ECTN data we can estimate the source spectrum for a range of azimuths exceeding  $270^\circ$ . A number of these data are at distances for which the *Lg* is the dominant phase. As noted by Shin and Herrmann (1987), the *Lg* phase at regional distances might actually be a more robust indicator of source properties than near-source data: it samples more of the focal sphere and provides a wide range of incident angles at receiver stations. For these reasons, we proceed in the rest of the paper to incorporate all of the SMA and ECTN data in an estimate of the source spectrum. (The NCEER data are excluded due to the low resolution at most stations, as discussed by Atkinson (1991).) This also allows us to determine the source spectra for the foreshock and aftershock, which were not recorded on the SMA stations.

#### ANALYSIS OF COMBINED DATA

##### *Data Processing*

Three-component data from the SMA network for the Saguenay mainshock were digitized and corrected for instrument response by Munro and Weichert (1989). Most ECTN stations record only the vertical component. The ECTN records were corrected for instrument response using the transfer functions provided by W. Shannon (personal comm., 1989) to obtain the Fourier acceleration spectra. For data from both the SMA and the ECTN stations, a tapered window with a duration of approximately 20 sec (longer for stations at greater distances) beginning at the onset of the *Lg* phase was used to window the strongest shaking. The optimal window length involves a trade-off between short durations, which give the best signal-to-noise ratio, and long durations, which are required to include all of the significant motion at large distances. Tests of the sensitivity of the spectra to the selected window length indicate that the selected window length is not a critical factor.

Noise is generally not an important consideration in the analysis of SMA data, due to the strength of the signal. For the ECTN data, however, care must be taken to ensure that an adequate signal-to-noise ratio is maintained for all analyzed data. This was accomplished through inspection of the noise spectrum for each record, obtained from a sample taken immediately before the *Lg*-wave onset.

The appropriate window selection for the analysis of noise warrants discussion. Analysis of the *Lg* phase is often confounded by the high-frequency *Sn* phase, and by the *P* coda. At close distances, the *Sn* phase is embedded in the

*Lg* signal, or precedes it by only a short time, so that the *Lg* phase begins within the *Sn* coda. At larger distances, there is a good separation of *Sn* from *Lg*, enabling *Lg* to be more easily isolated. When pre-*Lg* “noise” samples are taken such that much of the *Sn* phase is included, it appears that the high-frequency portion of the *Lg* spectrum (e.g., 3 Hz and above) is not significantly stronger than this “noise” signal. This is shown on Figure 4. Note, however, that in the frequency range 3 to 15 Hz the *Lg* spectrum does not rise with increasing frequency, as would be expected if it were contaminated by noise; note also that the “noise” spectrum actually exceeds the *Lg* spectrum for all frequencies above 3 Hz. These observations suggest that a pre-*Lg* noise sample that includes *Sn* overestimates the actual noise contained in the *Lg* signal. For this reason, one might choose to define the noise as that which precedes all seismic signal, accepting that in some distance ranges the *Lg* spectrum will contain some or all of the *Sn* phase.

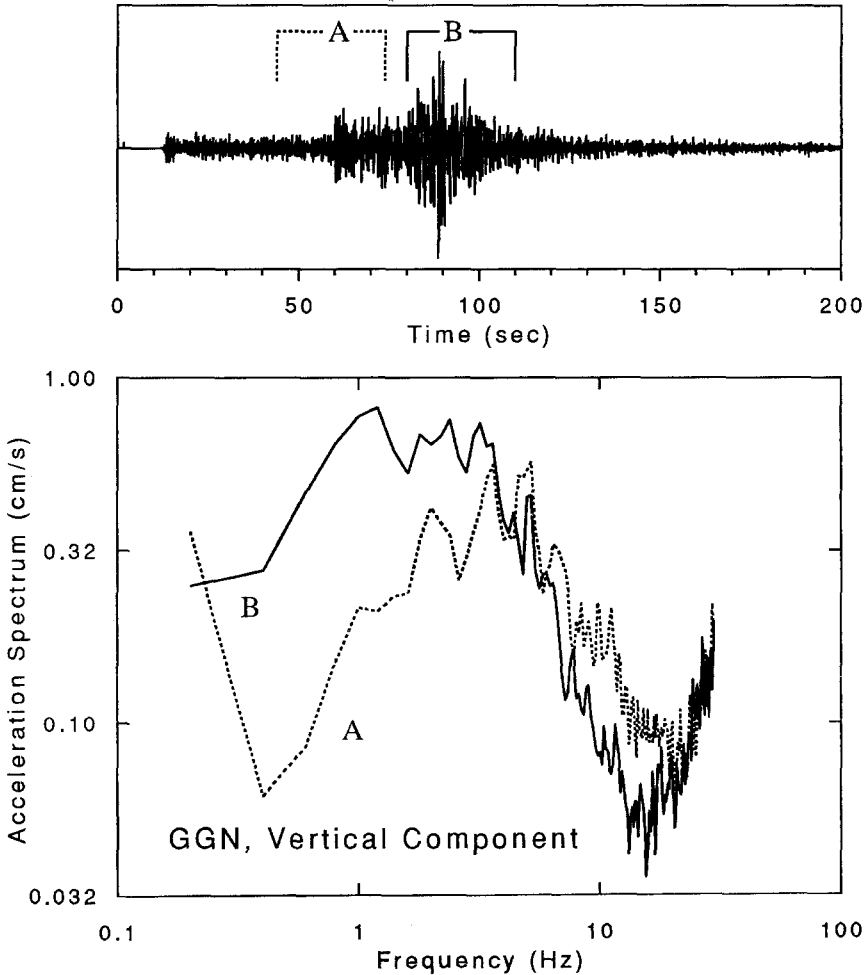


FIG. 4. Comparison of *P*-coda spectrum (dots) including *Sn* as shown in time window A with *Lg* spectrum (lines) as shown in time window B. Mainshock recorded at ECTN station GGN (472 km epicentral distance).

An additional consideration in selecting the noise window, however, is ensuring consistent treatment of *P*-coda noise in analyzing the *Lg* spectral levels. Figure 5 shows bandpassed seismograms from the foreshock at one of the ECTN stations. A high-frequency ringing persists from the *P* onset throughout the signal (this is more pronounced at some stations than at others). The low-frequency amplitudes of the *P* coda, by contrast, are small compared to those of the *Lg* phase. The use of a pre-*P* noise window therefore may lead to an overestimate of the *Lg* spectrum at high frequencies. To avoid this potential bias, we have opted to define the *Lg* noise window as that immediately preceding the *Lg* onset. This decision led to the elimination of many of the high-frequency data points, due to their contamination by *Sn* or the *P* coda.

Fourier acceleration amplitudes were computed for all records. The amplitudes were obtained by correcting the Fourier spectra of the recorded motions

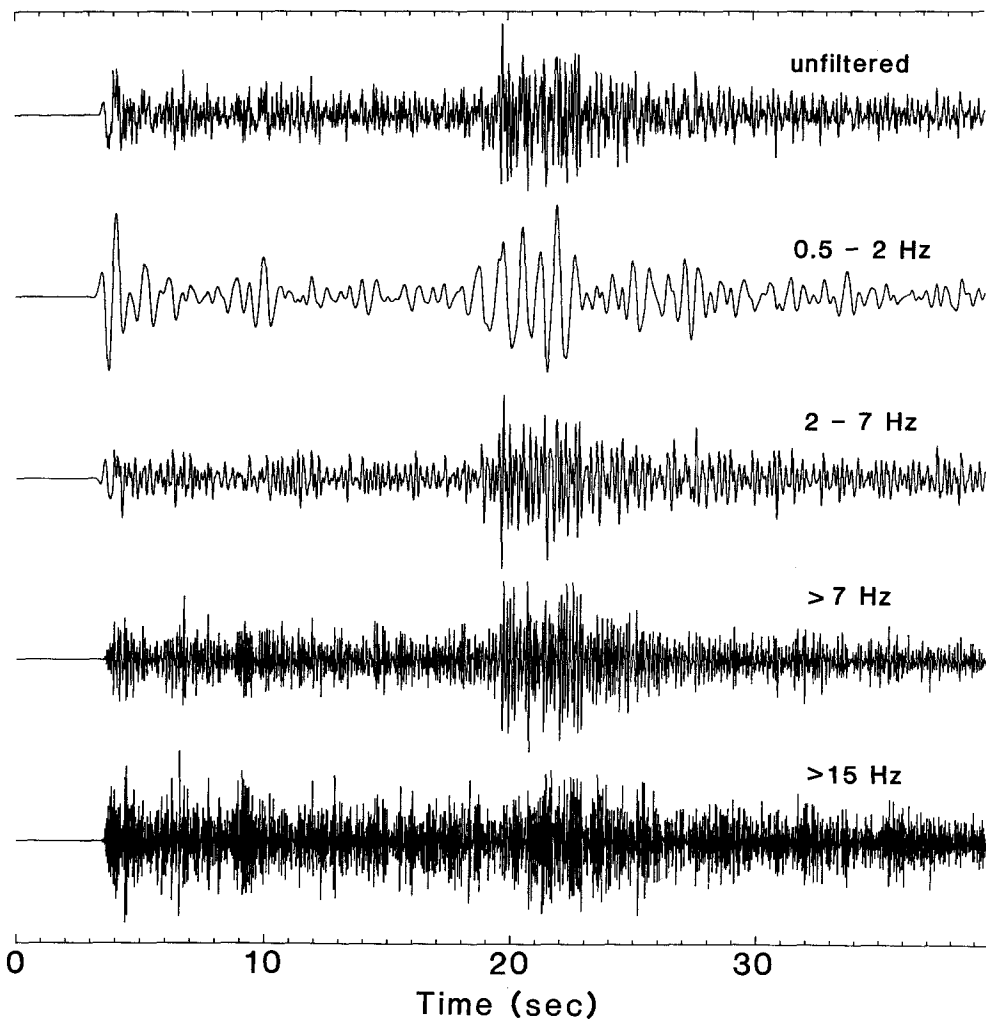


FIG. 5. Bandpass-filtered seismograms from foreshock recorded at ECTN station LPQ (123 km epicentral distance). Records show (from top to bottom): unfiltered velocity, 0.5 to 2, 2 to 7, > 7, and > 15 Hz. Traces have been individually normalized; vertical scale is unimportant for the purposes of this figure.

for the response of the instruments to ground acceleration. The correction factors, normalized to unity at 1 Hz, are shown in Figure 6 for the various systems used in the ECTN. We found in general that the corrected spectra were not trustworthy above the upper corner frequency for each response, and for that reason the spectra above that corner were not used in the analysis. The amplitudes were smoothed by applying a triangular smoothing function with 0.44 Hz half-width to the squared amplitude spectrum and then taking the square root of the result. Spectral values were read off the graphs at a series of seven frequencies equally spaced in log frequency (from 0.56 to 18 Hz). To minimize scatter in ground motion values due to inter-frequency variability (i.e., the locations of peaks and troughs of the spectra), some subjective smoothing of the spectra was done in the vicinity of the frequencies for which the spectral values were tabulated.

### Attenuation

Plots of the Fourier acceleration spectra as a function of distance suggested that the data may contain high- and low-amplitude subsets. This is not critical to the estimation of source spectra, which are intended to be an average over the focal sphere, but we discuss the issue briefly because it may have some geophysical significance. When plotted on maps (Fig. 7), the subsets appeared to be related to the source-to-station azimuth, with the contours elongated to the southwest. Hough *et al.* (1989) came to the same conclusion from their analysis of NCEER data. The intensity data (Drysdale, personal comm., 1990) also

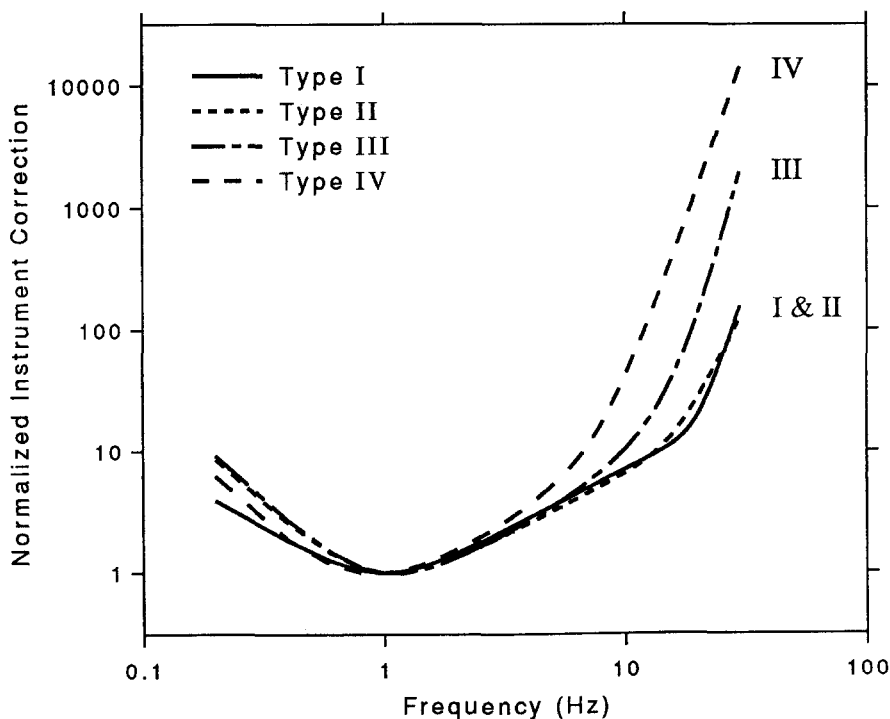


FIG. 6. The instrument correction factor (inverse response to ground acceleration) for the systems used by the ECTN. Most of the stations use system II.

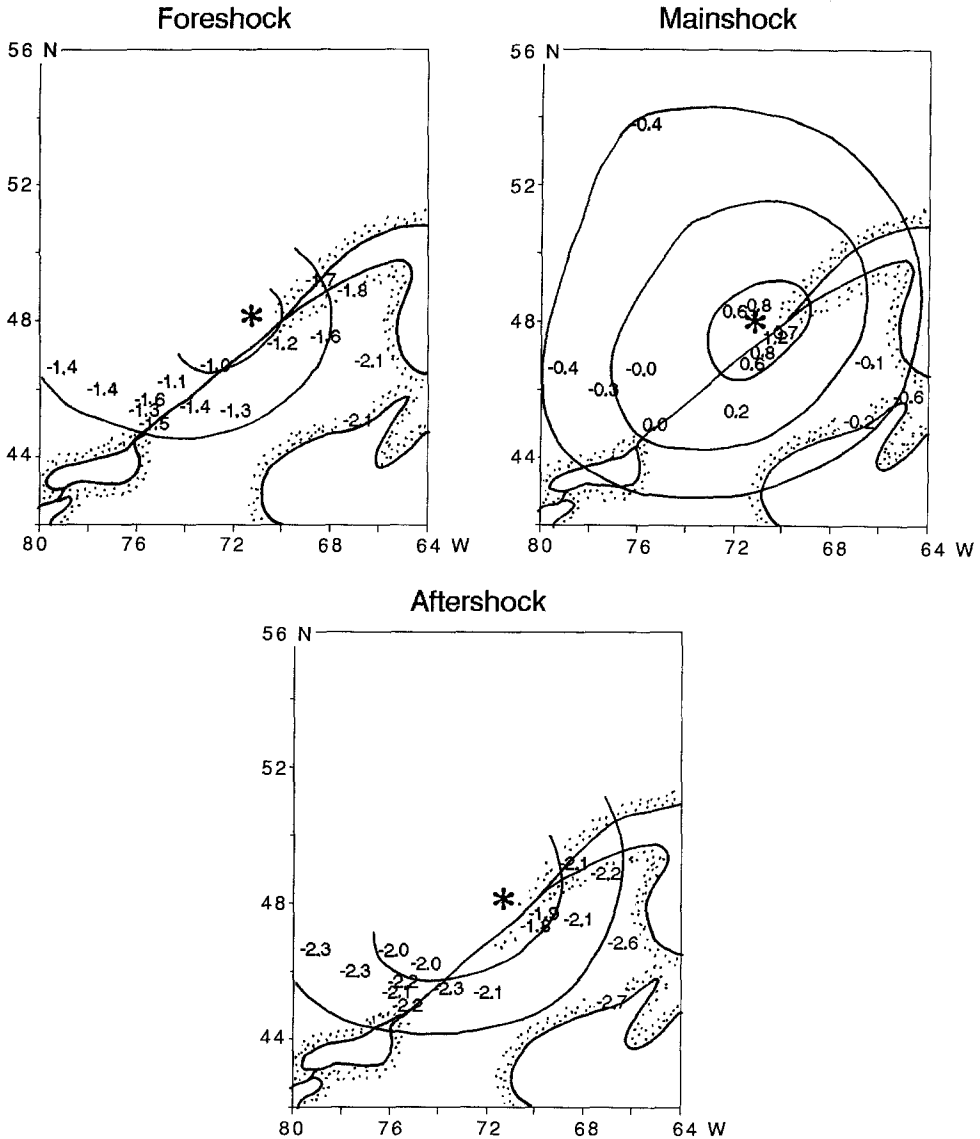


FIG. 7. Map of the logarithm of the 3-Hz Fourier acceleration spectra for the vertical component of ground motion for the mainshock, foreshock, and aftershock. The landward edge of the shoreline is stippled. The lines are speculative contours, at 0.5 log unit intervals. The nonisotropic radiation is apparent on these figures.

support the existence of an azimuthal dependence of amplitude for the mainshock.

It is tempting to attribute an azimuthal dependence to differences in attenuation. The subsets of amplitude seem to correspond to tectonic province, with the motions being larger in the Pre-Cambrian provinces, in which most of the stations are located, than in the Appalachian tectonic province to the southeast (the approximate boundary between the provinces is shown in Fig. 1). On the other hand, the smaller amplitudes correspond to waves traveling perpendicular to the structural grain of the St. Lawrence Valley (i.e., southeast and

northwest); studies of isoseismal maps of historical earthquakes suggest that the intensities are elongated in the direction of the structural grain (Armbruster and Seeber, 1987; D. Weichert, personal comm.).

Radiation pattern and source directivity, as well as wave propagation in purely elastic but laterally nonuniform media (including local site amplification or attenuation), can also cause apparent differences in attenuation. To distinguish between these effects requires many stations along various profiles radiating from the source, a requirement that is only partially met with the recordings of the Saguenay earthquakes.

We have plotted the Fourier acceleration spectra in Figure 8 for three of the seven frequencies used in our analysis; note that the amplitude differences between the data from the three events decrease with increasing frequency, in qualitative agreement with source theory. The filled symbols correspond to stations in the Pre-Cambrian tectonic provinces (primarily the Grenville

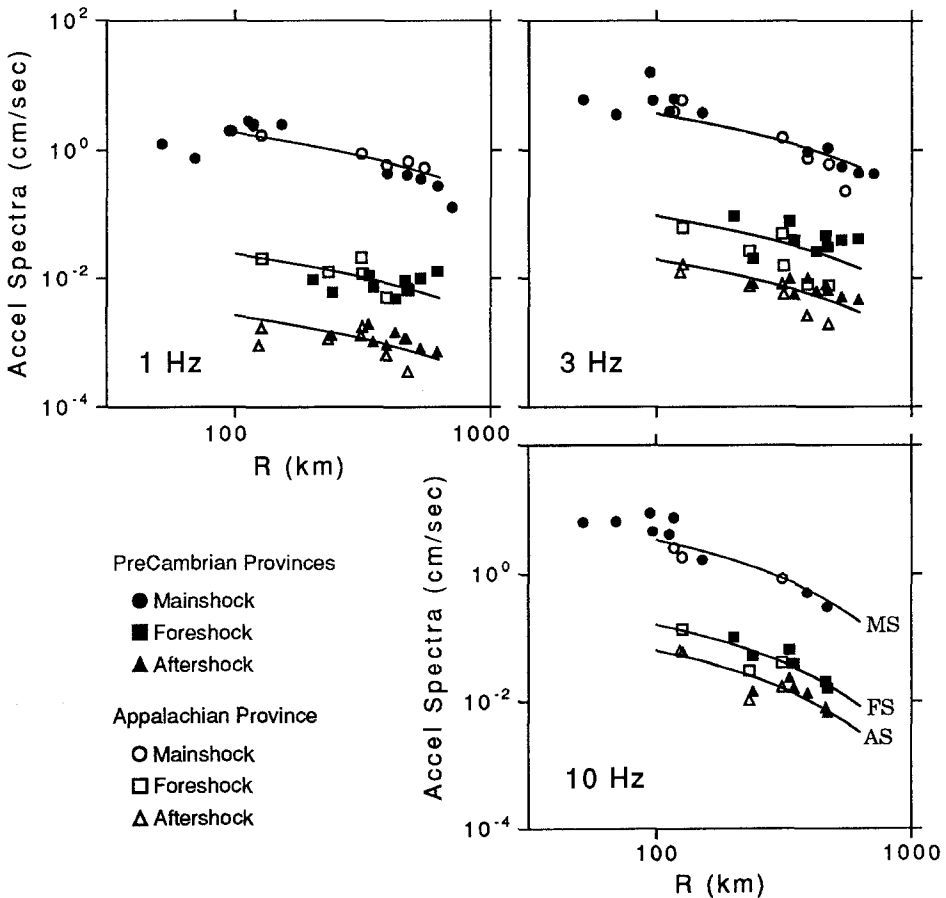


FIG. 8. Fourier acceleration spectra for the vertical component of ground motion for the mainshock (circles), foreshock (squares), and aftershock (triangles) as a function of hypocentral distance for three frequencies. The mainshock data include records from the SMA and ECTN networks; the spectra for the other events were obtained from ECTN records only (the SMA network did not record these smaller events). The lines show the attenuation curves fit to the combined data, using the model in equation (2). (Similar analyses were made for four other frequencies evenly spaced in log frequency.) Notice the decreasing separation between the curves as frequency is increased, in accord with seismological source theory.

province); the other data come from stations in the Appalachian province. The separation between data is most pronounced for the fore- and aftershocks at a frequency of 3 Hz, but overall it is arguable whether the differences are pervasive enough to warrant explicit treatment in the estimation of source spectra. We have lumped the data together in the analyses discussed in the rest of the paper.

The attenuation of the waves from the lumped data set has been determined by fitting the following model to the combined foreshock, mainshock, and aftershock data:

$$\log A_{obs} = a_1 \cdot FS + a_2 \cdot MS + a_3 \cdot AS - 0.5 \cdot \log R - k \cdot R, \quad (2)$$

where  $A_{obs}$ ,  $a_1$ ,  $a_2$ ,  $a_3$  and  $k$  are functions of frequency.  $FS$ ,  $MS$ , and  $AS$  are variables that take the value 1 if the data are from the fore-, main-, and aftershock, respectively, and 0 otherwise. The coefficient 0.5 is the geometrical spreading factor for surface waves; its application to the data regressions is supported by synthetic calculations described later. In order to measure the attenuation for a phase that nominally follows the same geometrical spreading relation, we used only data beyond 100 km in fitting the model. The resulting coefficients are given in Table 2 and the attenuation curves plotted in Figure 8. Residuals measuring the difference between the observed spectra and the model given by equation (2) are plotted as a function of azimuth and distance in Figures 9 and 10, respectively. Some systematic trends are apparent. For example, on the average the observed values are low for the fore- and aftershocks at azimuths between  $45^\circ$  and  $135^\circ$ , compared to the motions at azimuths between  $180^\circ$  and  $270^\circ$ . (This is, of course, consistent with the previous discussion of azimuthal changes.) The mainshock shows a different trend, with the largest motions being recorded at azimuths near  $180^\circ$ . This trend, which may be due to source directivity, is compromised by the trend with distance shown in Figure 10. Unraveling the various influences on the residuals is beyond the scope of the paper. The systematic trends revealed in Figures 9 and 10 are not such that they will impact our estimated source spectra in any important way.

For ease of comparison with other estimates of attenuation in the general region, the  $k$  values have been converted to  $Q$  using the equation in the footnote to Table 2. The values are plotted in the top panel of Figure 11, along with their 68% confidence limits. The frequency dependence of the attenuation

TABLE 2  
COEFFICIENTS FOR REGRESSIONS OF OBSERVED VERTICAL-COMPONENT FOURIER SPECTRA

$f$ (Hz)	$a_1$ (FS)	$a_2$ (MS)	$a_3$ (AS)	$k$ ( $\text{km}^{-1}$ )	$Q_{Obs}^*$	$Q_{Pred}^\dagger$	$\Delta Q(\%)$
0.6	-0.991	0.940	-1.951	0.000394	556	560	-1
1.0	-0.558	1.332	-1.522	0.000559	697	755	-8
1.8	-0.215	1.546	-1.056	0.000595	1165	1018	14
3.2	0.064	1.649	-0.622	0.000814	1515	1374	10
5.6	0.332	1.750	-0.219	0.001392	1575	1853	-15
10.0	0.378	1.704	-0.031	0.001682	2318	2500	-7
17.8	0.171	1.614	-0.143	0.001891	3666	3372	9

\* Calculated from  $Q = (\pi \log e)(f/(kv))$ , with  $v = 3.5$  km/sec.

† From  $Q = 755f^{0.52}$  (a least-square fit to the logarithm of the values in the column to the left).

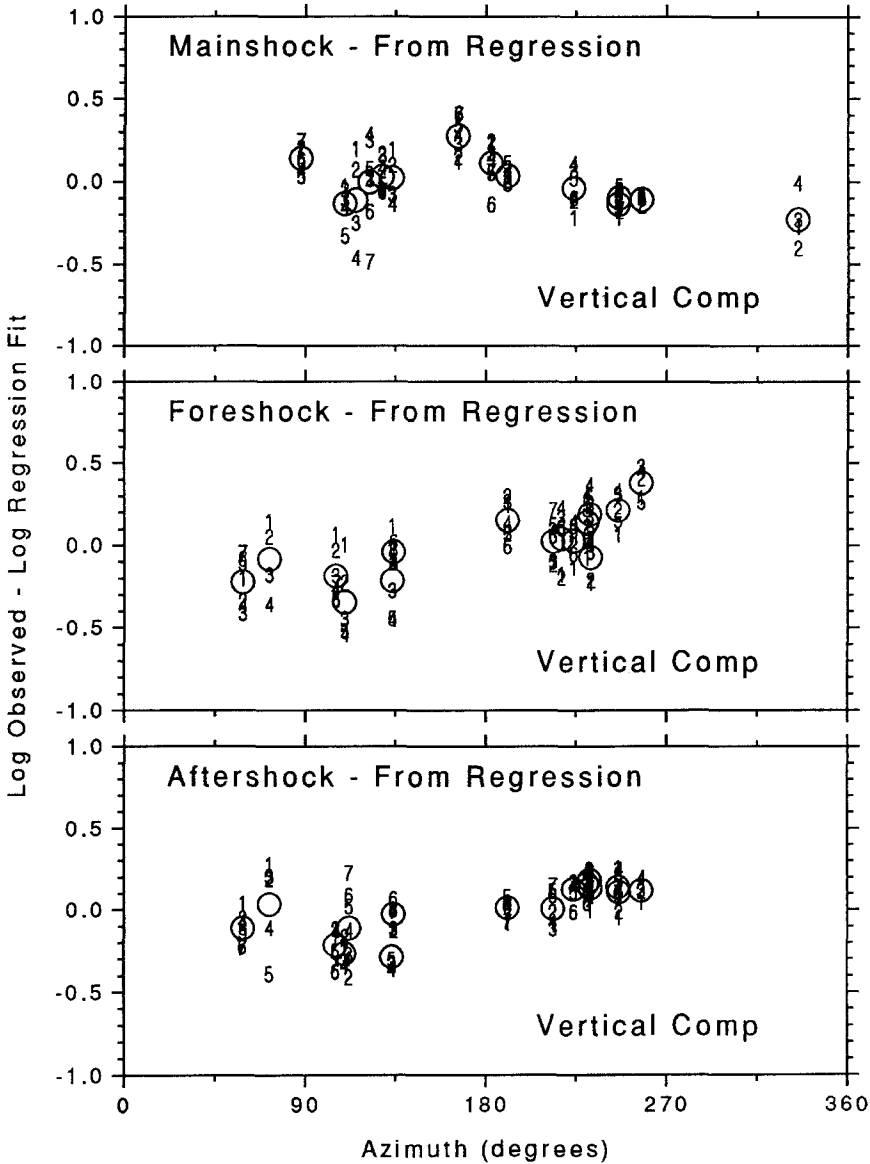


FIG. 9. The residuals of the data about the regression fits, plotted against source-to-station azimuth (clockwise from north). Only stations at distances beyond 100 km are included. The numbers indicate the frequency, increasing from 0.6 Hz for "1" to 17.8 Hz for "7" (the set of seven frequencies is given in the first column of Table 2); the circles are the averages of the residuals over frequency for each station.

is well described by the function  $Q = 755f^{0.52}$  (recall that this assumes a geometrical spreading of  $1/\sqrt{R}$ ). The derived  $Q$  function is consistent with, but somewhat larger than, most other measurements over similar travel paths (a mixture of Shield and Appalachian) in eastern Canada (*bottom panel*); the apparently higher  $Q$  may be attributable to the larger-than-average focal depth. The results are inconsistent with the Hough *et al.* (1989) determinations, which were based on the NCEER data from the Saguenay earthquake. We suspect that this difference is due to the sensitivity of their results to the

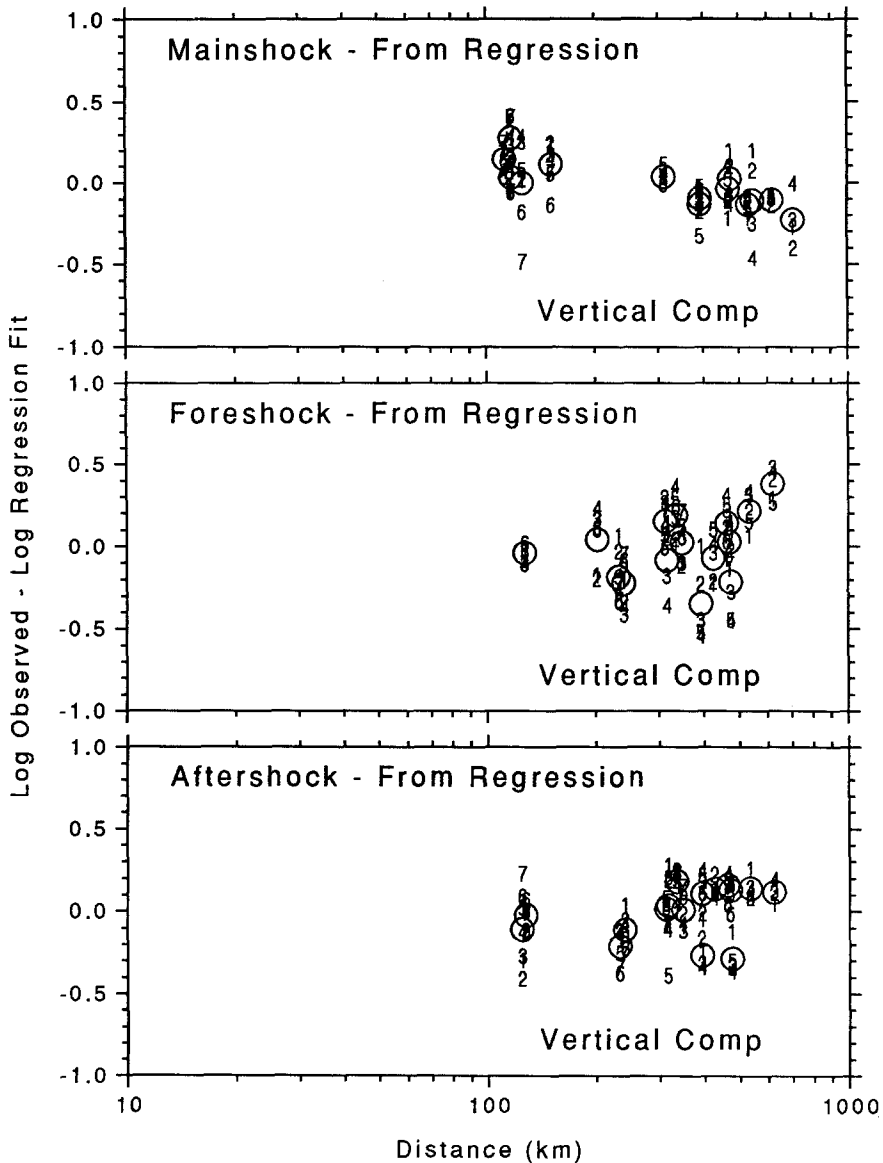


FIG. 10. The residuals of the data about the regression fits, plotted against hypocentral distance. The abscissa starts at 10 km for ease of comparison with a later figure for which data at less than 100 km are plotted. The numbers indicate the frequency, increasing from 0.6 Hz for "1" to 17.8 Hz for "7" (the set of seven frequencies is given in the first column of Table 2); the circles are the averages of the residuals over frequency for each station.

amplitudes at the closest NCEER station (DCKY). DCKY is about 200 km from the source, and the next nearest station is over 300 km from the epicenter. Furthermore, DCKY was used in the  $Q$  determination for both subsets of their data. If the spectral amplitudes at DCKY are anomalously large relative to the rest of the data set, then their  $Q$  values would be biased downward (a point recognized by Hough *et al.* in their paper). This seems to be the case, as evidenced by the fact that the DCKY amplitudes are significantly larger than those from several GSC stations at comparable distance and azimuth (e.g., Fig. 2).

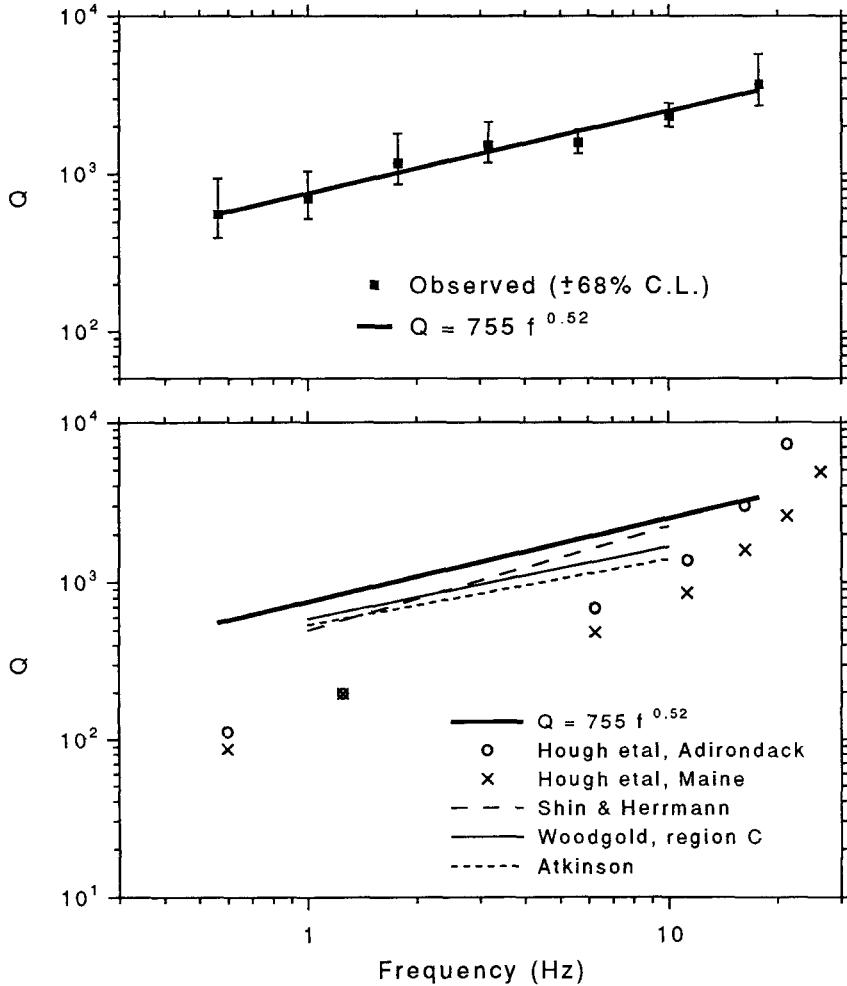


FIG. 11. Measured attenuation as a function of frequency. The *top panel* shows the  $Q$  values determined in our study (see Table 2), along with the least-square fit of a straight line to the data. The error bars are 68% confidence limits of  $Q$ . The *bottom panel* compares our results (heavy solid line) with those of several other studies for similar travel paths (a mixture of Shield and Appalachian) (Shin and Herrmann, 1987; Atkinson, 1989; Hough *et al.*, 1989; Woodgold, 1990).

### Ratio of Horizontal to Vertical Spectral Amplitudes

Most ECTN stations recorded only the vertical component of ground motion; for this reason the regressions were based on vertical component data. Horizontal component data are available, however, from the SMA network for the mainshock and from ECTN stations GAC and Axx (where the "xx" represents the number of the station in the Charlevoix array, which we consider to be part of the ECTN) for the fore- and aftershock. These data can be used to derive the horizontal-to-vertical component ratio ( $H/V$ ) needed in some comparisons of the vertical data to theoretical predictions for the horizontal component. Furthermore, these results were used in estimating the response spectra shown in Figure 2. The ratios were computed from Fourier amplitude spectra, using  $\sqrt{(H_1^2 + H_2^2)2}$  as the measure of the horizontal spectra ( $H_1$  and  $H_2$  are the spectra of the two horizontal components). For each frequency, the logarithms of

the ratios were averaged over all stations. No systematic trends were found when the ratios from individual stations were plotted against distance for each earthquake separately (which gives some assurance that the attenuation of *Lg* waves is similar for spectral amplitudes computed from vertical and horizontal components, an assumption made in some of the later analyses). The computed *H/V* ratios for all three-component stations are shown as a function of frequency (of the Fourier amplitudes) on Figure 12. Results are shown for both unsmoothed and smoothed data, where the smoothing was over the square of the amplitude spectra for each component (and therefore before division to form the ratio). Also shown in Figure 12 are lines representing the *H/V* ratio of 1.4 assumed in the ground motion relations of Atkinson and Boore (1990) and a quadratic fit to the ratios obtained from smoothed spectra. The quadratic fit gives the equation

$$H/V = 1.14 + 0.118f - 0.00638f^2 \quad (3)$$

for the ratio of horizontal-to-vertical ground motion. The observed ratio is slightly lower than 1.4 for frequencies less than 4 Hz, and slightly higher for greater frequencies. The increasing size of the horizontal component relative to

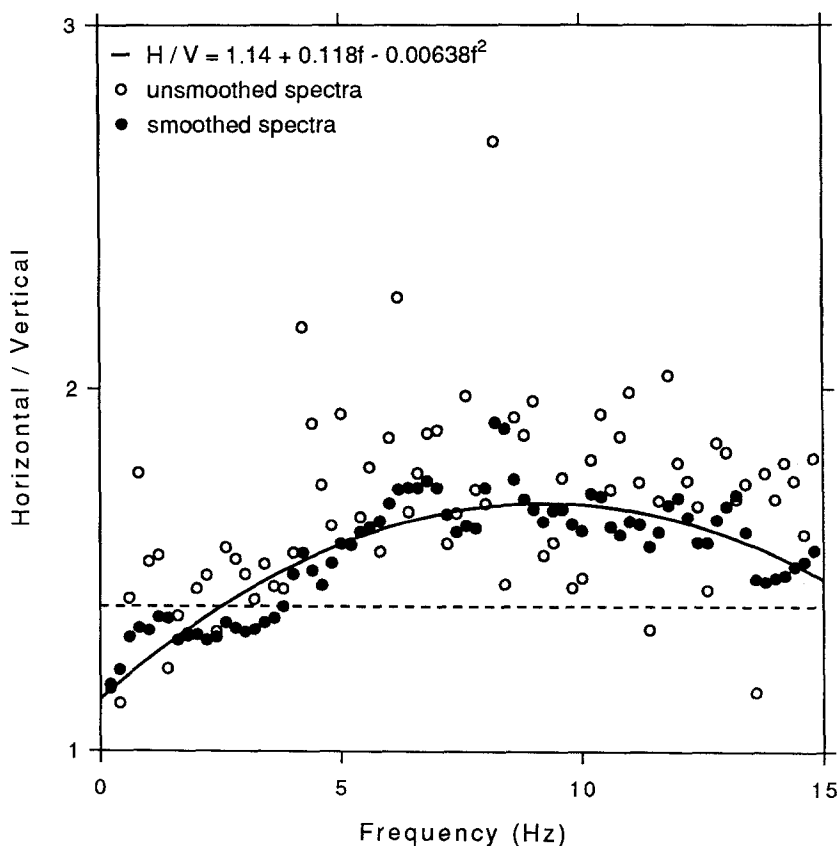


FIG. 12. Observed *H/V* ratios for Saguenay data. Filled circles are based on smoothed horizontal and vertical spectra; circles use unsmoothed spectra. The dashed line shows *H/V* ratio of 1.4, and the solid line shows quadratic regression fit to data.

the vertical component as the wavelength is decreased may be due to the presence of lower velocity materials close to the surface (R. Herrmann, written comm., 1991). If so, the lack of systematic differences between the widely separated stations used to determine  $H/V$  argues that the low-velocity materials are not unique to one site.

### *Estimation of Source Spectra*

To make a quantitative assessment of the source spectra requires some way of extracting the source spectra from the observed spectra (most of which are for *Lg* waves). We present three approaches. The first (method 1), and the simplest, assumes  $1/R$  geometrical spreading over all distances and a uniform medium. The second and third methods both use synthetic seismograms to account for the source excitation and propagation for an earth structure in which the velocity and density vary with depth (but not laterally). The latter two methods differ from each other in the way that averages are taken over distance and azimuth: method 2 uses the synthetic seismograms at the specific distance, azimuth pairs corresponding to the observations to make estimates of the source spectrum for each site; method 3 averages both the synthetic seismograms and the observations over distance and azimuth before extracting the source spectrum. In all cases, we are attempting to estimate a source spectrum that is an average over the focal sphere, for such an average spectrum is of direct use in estimating average ground motion parameters.

*Method 1: Uniform Media,  $1/R$  Spreading.* A number of studies have found that the shapes of the amplitude spectra for *Lg* waves are unaffected by propagation effects, and that the simple formula in equation (1) can be used to relate the *Lg* spectra and the source spectra (Street *et al.*, 1975; Herrmann and Kijko, 1983; Campillo *et al.*, 1984; Ou and Herrmann, 1990). Thus regression analysis of the combined SMA and ECTN data may be used to simultaneously determine source levels and attenuation parameters, as in Atkinson (1989). We fit the vertical-component data for the three events simultaneously, assuming that the spectral amplitudes decayed with a geometrical spreading of  $R^{-1}$  and an anelastic attenuation of the form  $10^{-k'R}$ , using data at all distances. Note that we represent the anelastic attenuation by the coefficient  $k'$  rather than the  $k$  used earlier;  $k$  was associated with the assumption of  $1/\sqrt{R}$  geometrical spreading, which is generally considered appropriate for distances greater than 100 km. The  $1/R$  spreading was imposed as a computational convenience in handling both direct-wave and *Lg*-wave data in a simple regression format. Atkinson (1989) found that  $1/R$  spreading could be justified for the *Lg* data because the scatter in the data does not allow a distinction between a steep slope with gentle curvature and a gentle slope with pronounced curvature. Furthermore, the ground-motion predictions were not strongly dependent on the assumed form.

The inversion of the Saguenay data was done frequency by frequency. For each frequency, the coefficient  $k'$  was used to correct for the effect of anelastic attenuation, and the corrected intercepts of the regression equations were used in equation (1) to obtain the source spectrum  $S_a(f)$ . The spectral amplitudes for the vertical component were multiplied by  $H/V$  factors given by equation (3) to approximate the estimates that would have been obtained from horizontal-component spectra. The results are presented in a later figure comparing the outcome of the three methods of estimating the source spectrum.

Because of the azimuthal dependence of attenuation, the regressions investigated the effects of subdividing the data into sets parallel ( $\pm 30^\circ$ ) and perpendicular ( $\pm 30^\circ$ ) to the St. Lawrence, as well as the effect of using just the data from Grenville Province travel paths (there are not enough Appalachian path data for a meaningful regression). The results from the subdivided data sets are similar to those obtained using the entire set. Similar results were also obtained for an assumed geometrical spreading factor of  $1/\sqrt{R}$  for distances greater than 100 km.

*Wave Propagation in a Layered Earth (Methods 2 and 3).* There are several questions concerning method 1 that have motivated us to develop two other methods for the extraction of the source spectrum from observed spectra. These questions are: (1) In view of the complications introduced by wave propagation in a layered crust (e.g., Somerville *et al.*, 1990), is it valid to use a simple power law to extrapolate distant observations back to the source? (2) Does the source depth (about 28 km for the Saguenay events) compromise the relationship between  $L_g$  amplitudes and source amplitudes? This latter question arises because the previous studies documenting such a relationship were for shallower sources. More recent studies (Gariel and Jacob, 1989; Ou and Herrmann, 1990) considered sources as deep as 30 km and found a dependence of the inferred spectral level on source depth.

An alternative method of projecting the observed spectra back to the source is to base the relation between the observed and the source spectra on synthetic seismograms. We pursued this approach, using a reflectivity program (provided by Harley Benz), with the crustal structure model and mainshock focal mechanism of Somerville *et al.* (1990). A step-function source with a nominal moment of  $1.0 \times 10^{20}$  dyne-cm was assumed for all simulations. This source spectrum is not intended to model the Saguenay source. The step-function source was selected because it allows a simple determination of how the amplitudes propagate with distance; this is all that matters for our purposes. Three-component seismograms were calculated for a source at 26 km and azimuths and distances corresponding to the stations providing data from the mainshock. In addition, we computed the motions for two profiles at azimuths of  $0^\circ$  and  $45^\circ$  clockwise from north. For the sake of comparison, we also generated the motions for a source at a depth of 5 km.

For each time series, the Fourier spectra were computed for the dominant motion. Plots of the spectra indicate that wave propagation produces little frequency dependence in the spectra: the spectral level remains essentially flat from 1 to 10 Hz, as it would be in a whole space of uniform velocity (this finding has been noted by others, e.g., Herrmann and Kijko, 1983; Campillo *et al.*, 1984). A typical example is given in Figure 13.

*Method 2: Estimation from Individual Stations.* The spectral level of the synthetic seismograms provide a direct calibration of the source excitation, radiation pattern, wave propagation, and free-surface effects that can be used to estimate the source spectra from the individual observations (including partitioning of the energy into vertical and horizontal components). In equation form,

$$\frac{A'_{obs}(f)}{D_{syn}} = \frac{S_a(f)}{10^{20}}, \quad (4)$$

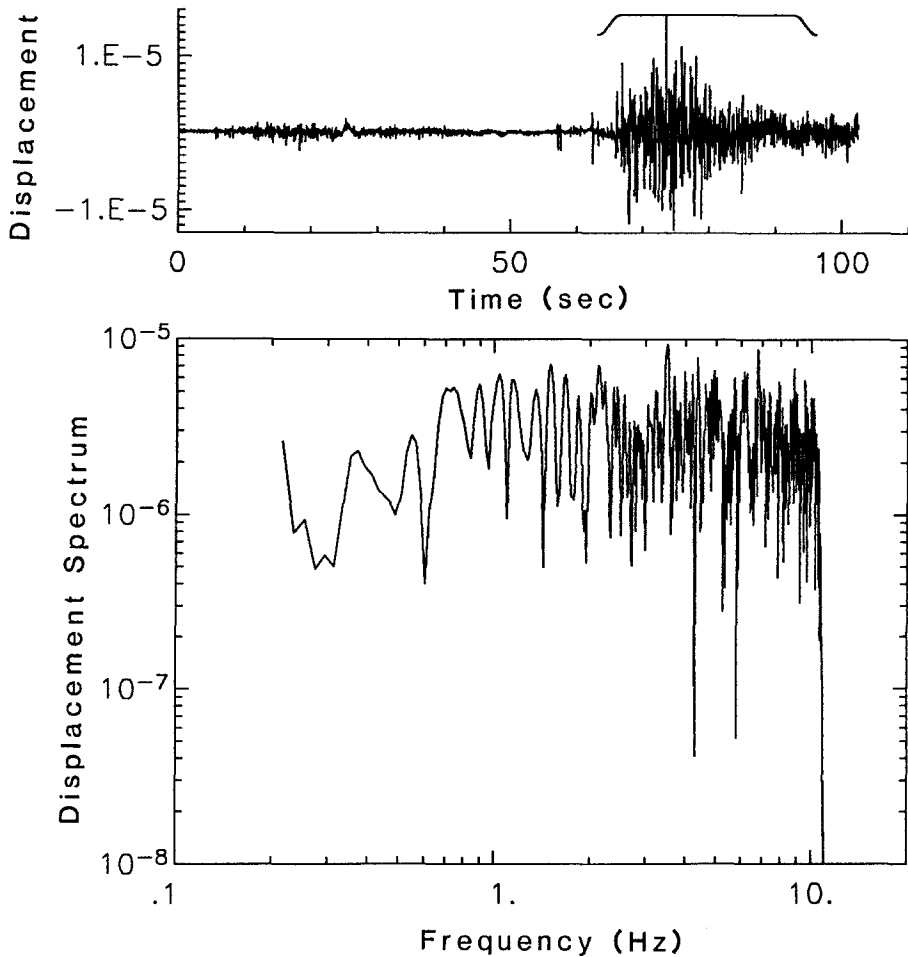


FIG. 13. Displacement time series and Fourier spectrum for the portion of the time series indicated by the bracket. The time series is a synthetic seismogram at 467 km. The source-time function was chosen so that the spectrum in a uniform whole space would be flat. Note that the spectrum of the calculated motion is essentially flat between about 0.7 and 10 Hz, implying that wave propagation produces little distortion in the spectrum. (The spectrum was cut off at 10 Hz, a limit imposed by the synthetic seismogram calculations.)

which can be solved for  $S_a(f)$ . In this equation,  $D_{syn}$  is the frequency-independent spectral level of the synthetic ground displacement at the azimuth and distance of the station providing the data  $A'_{obs}$ . The factor  $10^{20}$  is the seismic moment, in dyne-cm, of the source used in the synthetic seismogram calculations. The calculations were for perfectly elastic media, and therefore a correction for anelasticity has been applied to the observed spectral amplitudes  $A_{obs}(f)$ , using the following equation:

$$A'_{obs}(f) = A_{obs}(f) \times 10^{k(f)R}, \quad (5)$$

where the frequency-dependent anelastic coefficient  $k(f)$  was determined by the regression analysis discussed earlier (equation 2, Fig. 8, and Table 2). Combining equations (4) and (5) gives

$$\log S_a(f) = 20 + \log A_{obs} + k(f)R - \log D_{syn}. \quad (6)$$

To apply equation (6), we computed  $D_{syn}$  by averaging the smoothed Fourier spectra for the appropriate time series over the frequency band 1 to 10 Hz. The values of  $D_{syn}$  are plotted in Figure 14, and Figure 15 contains the source spectra derived from individual stations and from the average at each frequency over the individual station estimates.

The radiation pattern and changes in amplitude due to critical-angle reflections have been included in the synthetic seismograms. If they reproduce the actual effects for the Saguenay earthquake, then a plot against azimuth of the residuals between the source spectrum computed for each station and the average source spectrum should reveal source directivity effects (such effects have been proposed for the Saguenay earthquake by Haddon (1992)). We show such a plot in Figure 16. An azimuthal variation does seem to be present, with high values at an azimuth of about  $135^\circ$  for the vertical component and  $180^\circ$  for the horizontal components, and low values at  $17^\circ$  for both the vertical and horizontal components. The degree to which the radiation pattern and wave propagation have been accurately accounted for by the synthetic seismograms is difficult to assess, but the residuals against distance shown in Figure 17 suggest that we have not been completely successful in this regard. The source spectrum estimates from the cluster of data at distances beyond about 300 km (all from ECTN stations) are systematically low relative to the estimates from closer stations (all from the SMA network). This may be due to the choice of the attenuation coefficient  $k$  (see Figs. 8 and 10). To get a sense of how this bias affects the azimuthal variation, we have indicated the residuals from the more distant stations with x's in Figure 16. Shifting these points upward by about 0.3 log units (the approximate bias from Fig. 17) would decrease the azimuthal variation (ignoring the unusually low value at  $17^\circ$ ).

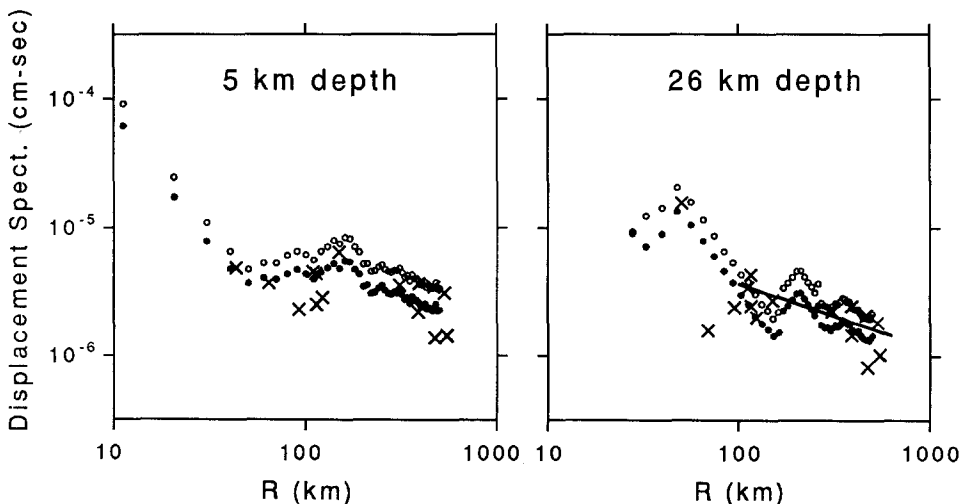


FIG. 14. Fourier spectra for windows encompassing the dominant motion in synthetic vertical ground motions, as a function of hypocentral distance. The ground motions were computed along profiles with azimuths of  $0^\circ$  (due north, filled circles) and  $45^\circ$  east of north (circles), as well as for distance and azimuths for which data were obtained in the mainshock (X's). The synthetics used the crustal model and focal mechanism of Somerville *et al.* (1990). A step displacement source-time function, with a moment of  $1.0 \times 10^{20}$  dyne-cm, was placed at depths of 5 and 26 km. The ordinate is the average from 1 to 10 Hz of the square root of the displacement spectrum (squared and smoothed over a 0.4-Hz smoothing window). This processing best approximates the smoothing done to the actual data.

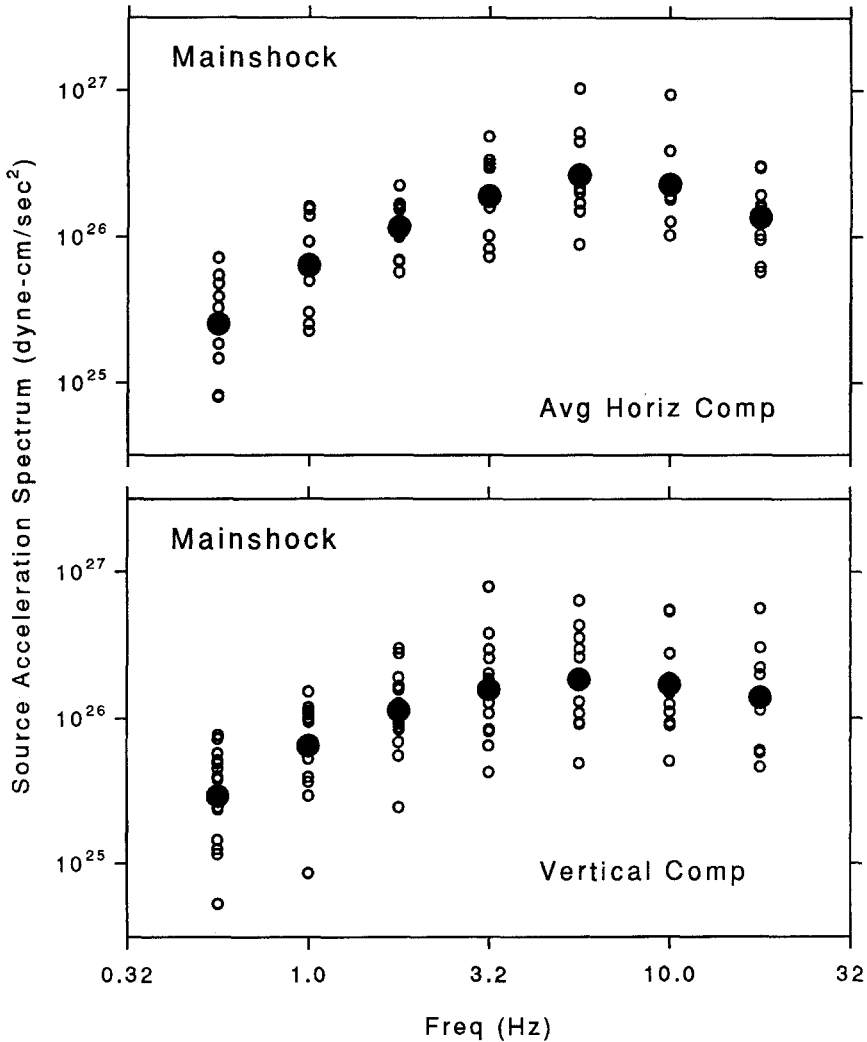


FIG. 15. Source acceleration spectra (as defined by equation B1) for the mainshock, using vertical component (SMA and ECTN data) and horizontal component data (SMA data). The horizontal component data are the average of the logarithms of the individual components. The synthetic seismograms computed for the azimuth and distance for each station (X's in Fig. 14) were used to correct the observed spectra for radiation pattern, source excitation, wave propagation, and free-surface interaction effects. The estimates from individual stations are given by the small circles; the averages of the logarithms of the individual stations are indicated by the large filled circles.

*Method 3: Estimation from Averages over Stations.* The method embodied in equation (6) for extracting the source spectrum from the observed spectrum puts a large premium on the correctness of the focal mechanism and velocity model used in the calculations. In particular, the synthetic values plotted in Figure 14 indicate that large variations occur in the motions for stations within small distance ranges. These variations are due to differences in the radiation pattern. Also noticeable are the changes over larger distance ranges, due to the arrival of waves critically reflected from the major crustal discontinuities. As others have pointed out (e.g., Somerville *et al.*, 1990; Bowman and Kennett, 1991), these reflections can lead to nonmonotonic decay of the peak ground

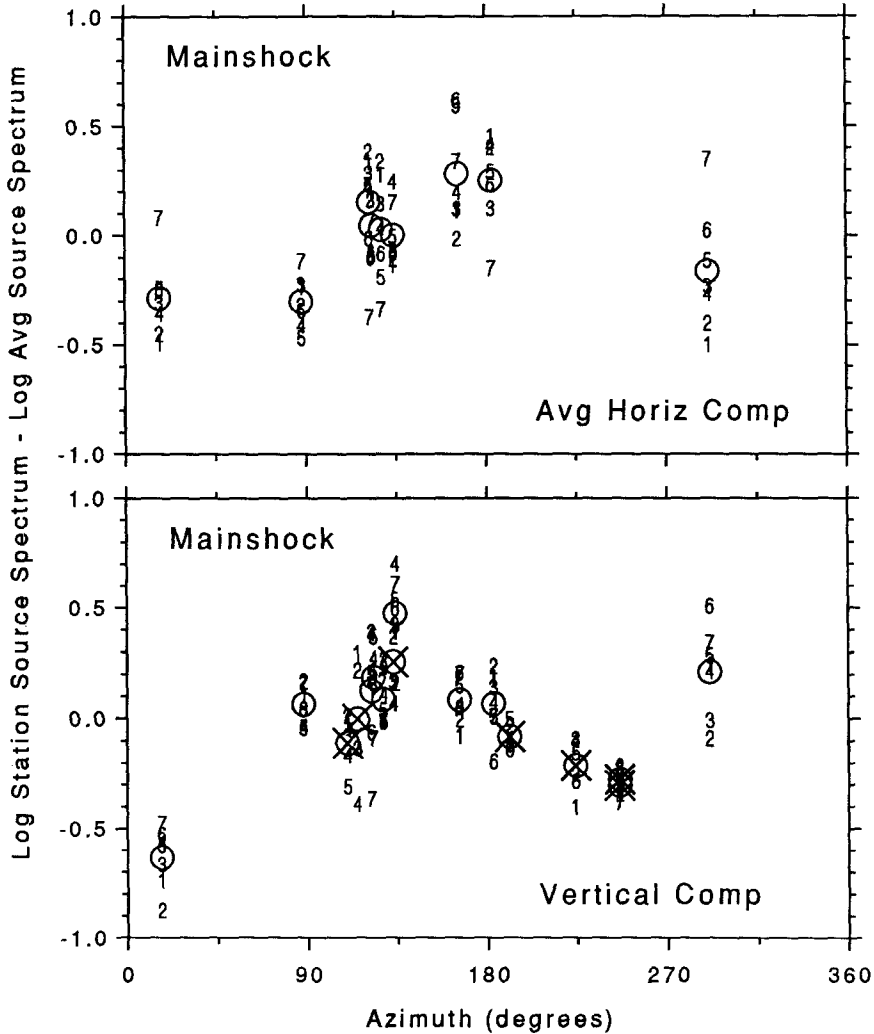


FIG. 16. Residuals (log of source spectrum estimated at a particular frequency and station minus the log of the average source spectrum) plotted against source-to-station azimuth (clockwise from north). Unlike Figure 9, the synthetic seismograms calculated at each station's azimuth and distance were used in extracting the source spectrum from the observed spectrum. The numbers indicate the frequency, increasing from 0.6 Hz for "1" to 17.8 Hz for "7" (the set of seven frequencies is given in the first column of Table 2); the circles are the averages of the residuals over frequency for each station, and the x's indicate those stations beyond 300 km.

motion, even for the *Lg* phase. One way to blunt the sensitivity of the synthetic seismograms to the particular focal mechanism and crustal structure would be to perform a Monte Carlo experiment, varying the parameters within a specified distribution function. This is a computer-intensive and costly exercise and is not warranted for the purposes of this paper. We have taken a simpler approach that averages out, to some extent, the variations in ground motion produced by the crustal structure and the radiation pattern. As seen in Figures 8 and 14, the spectral levels beyond 100 km can be approximated by a simple monotonic attenuation law. For this reason, for method 3 we use data only at distances beyond 100 km (unlike methods 1 and 2 for extracting the source

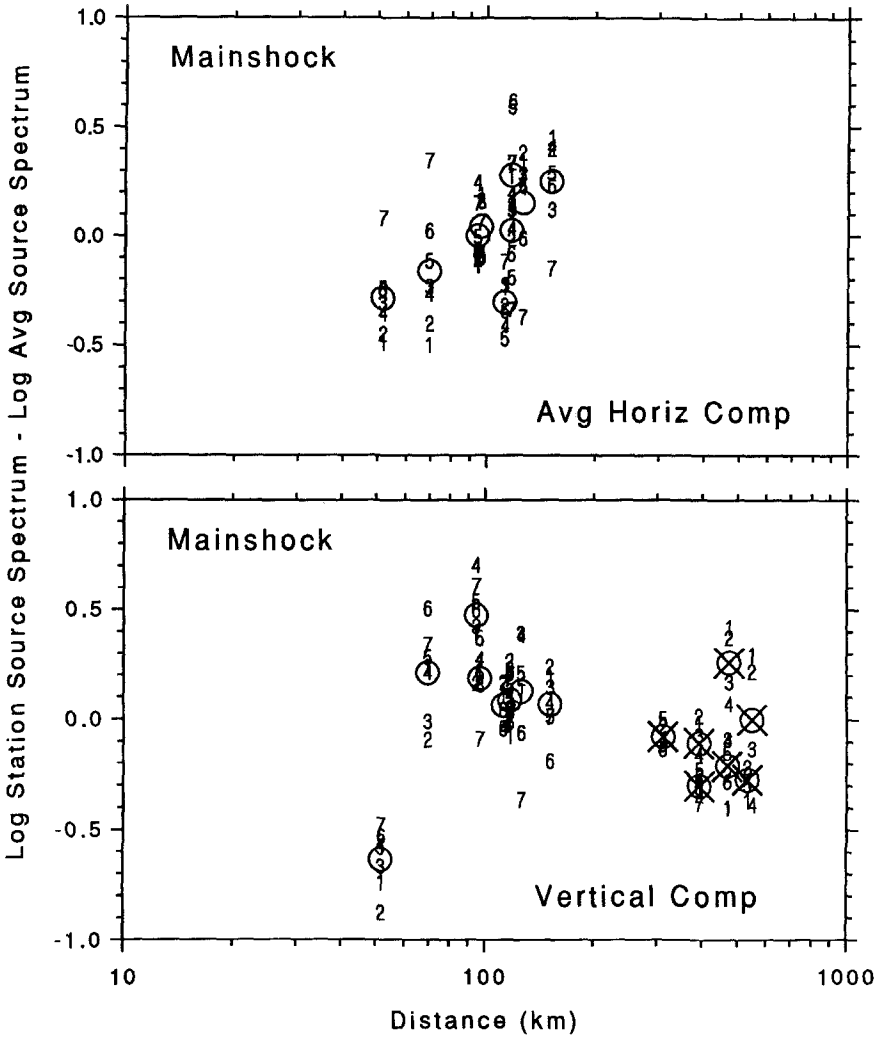


FIG. 17. Residuals (log of source spectrum estimated at a particular frequency and station minus the log of the average source spectrum) plotted against hypocentral distance. Unlike Figure 10, the synthetic seismograms calculated at each station's azimuth and distance were used in extracting the source spectrum from the observed spectrum. The numbers indicate the frequency, increasing from 0.6 Hz for "1" to 17.8 Hz for "7" (the set of seven frequencies is given in the first column of Table 2); the circles are the averages of the residuals over frequency for each station.

spectrum, which use data from all distances). The inherent assumption is that the positive residuals that would be expected in some distance ranges will be averaged out by the low residuals from other distance ranges, to obtain the correct average source spectrum. Therefore, the observed spectral levels can be fit to equation (2), with coefficients given in Table 2. Now assume that the spectral levels from the synthetic data can be described by the equation

$$\log D_{syn} = d - 0.5 \cdot \log R \tag{7}$$

(recall that no attenuation was included in the theoretical model, and therefore the factor  $k$  does not enter this equation). This equation has been fit to the

spectral levels in Figure 14, for data beyond 100 km. The value  $d$ , determined by combining all the synthetic data (the resulting line is shown in Fig. 14), is  $-4.434$ . Combining equations (2), (4), (5), and (7) gives the following equation for the source acceleration spectrum:

$$\log S_a(f) = 20 + a_1(f) \cdot FS + a_2(f) \cdot MS + a_3(f) \cdot AS - d. \quad (8)$$

The resulting estimates of the source spectra for the foreshock, mainshock, and aftershock are shown in Figure 18. This figure also contains theoretical fits (discussed later) and the estimates from the method assuming  $1/R$  geometrical spreading and uniform media (method 1) and the method based more closely on the synthetic seismograms (method 2). The bars indicate 68% confidence limits, primarily controlled by the uncertainty in the regression coefficients  $a_1$ ,  $a_2$ , and  $a_3$ . The source spectra from method 3 were estimated using vertical component data only, for not many horizontal component spectral levels are available for distances beyond 100 km.

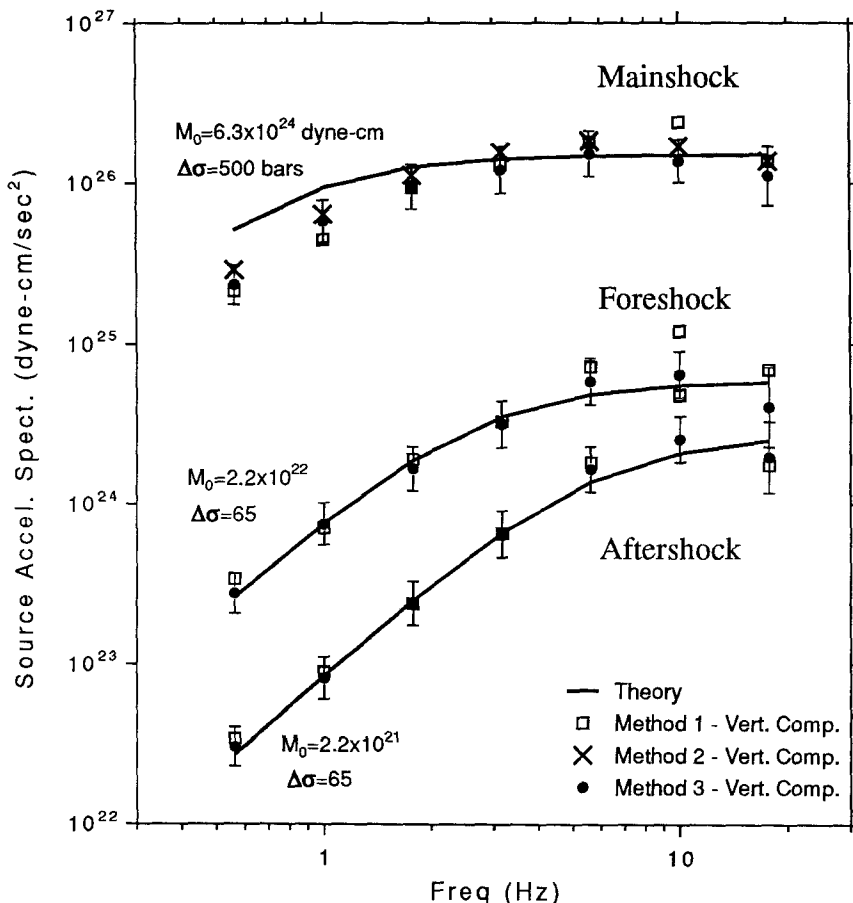


FIG. 18. Source acceleration spectra for the three events studied in this paper, based on vertical component data, compared with theoretical spectra. Three methods were used to extract the source spectra from the data (see text for full descriptions): Method 1 used the uniform whole space model (equation 1); method 2 used the ratio of observed and synthetic spectra at individual stations; in method 3 the observed and synthetic spectra were averaged over distance and azimuth before the source spectra were estimated.

An important conclusion from Figure 18 is that the source spectra derived under simple assumptions about source excitation and wave propagation are similar to those based on the more complicated synthetic seismogram correction approach. The agreement is striking, considering the very different nature of the analysis methods and the number of factors which a simple regression necessarily neglects. This result gives confidence that the derived spectra are robust and demonstrates that simple regression of data from regional distances can provide reliable source spectral estimates.

#### DISCUSSION

The source spectra estimated for the earthquakes are intended to represent an average over the focal sphere; the actual radiation would vary with azimuth and take-off angle because of radiation pattern and source directivity. The various estimates of the spectrum shown in Figures 15 and 18 are similar to one another and give us confidence that our estimates are a good representation of the overall radiation from the earthquakes. Within the uncertainty in the estimations, the acceleration spectra for all the events approach a level value, as expected for an  $\omega^{-2}$  source model, for frequencies above about 2, 4, and 6 Hz for the mainshock, foreshock, and aftershock, respectively.

#### *Modeling the Source Spectra*

The spectra for the foreshock and the aftershock can be well modeled by an  $\omega^{-2}$  spectra with a single corner frequency, as shown in Figure 18. For the mainshock, the observations do not extend to low enough frequencies to reach a conclusion in this regard (i.e., we cannot observe the  $\omega^2$  portion of the acceleration spectrum). The theoretical fits in Figure 18 are based on the equations for the Brune model, given in Appendix B, which have seismic moment ( $M_0$ ) and stress ( $\Delta\sigma$ ) as parameters. For the mainshock, we used  $M_0$  from the teleseismic observations ( $6.3 \times 10^{24}$  dyne-cm) and adjusted  $\Delta\sigma$  to match the high-frequency level (the required  $\Delta\sigma$  was 500 bars). For the fore- and aftershocks no independently determined seismic moments are available, but sufficient bandwidth is available for us to determine both  $M_0$  and  $\Delta\sigma$  by trial and error; the resulting values are shown on the figure.

The theoretical spectrum for the mainshock significantly overestimates the observed spectrum at frequencies near 1 Hz. This confirms our initial analysis of the source spectrum based solely on the record at SMA station S16. The stress parameters for both the fore- and aftershock have a value of 65 bars, which is much lower than that required to fit the mainshock spectra (500 bars).

The apparent lack of energy at intermediate frequencies for the mainshock source spectrum is intriguing. A more complete view of the source spectrum for the mainshock is obtained by combining our results with those of Boatwright and Choy (1992). They determined the source spectrum for the Saguenay mainshock from teleseismic  $P$  waves and provide estimates at lower frequencies than are available from the regional data. Their result is shown in Figure 19, along with the spectrum inferred by the three methods we have used to extract the source spectrum from the observed spectra. Boatwright and Choy's spectrum and ours overlap somewhat in frequency and are reasonably consistent in the region of overlap. Figure 19 also contains the theoretical spectra for the  $\omega^{-2}$  model, using the independently determined seismic moment for the earthquake and two values for the stress parameter (100 bars, used in our

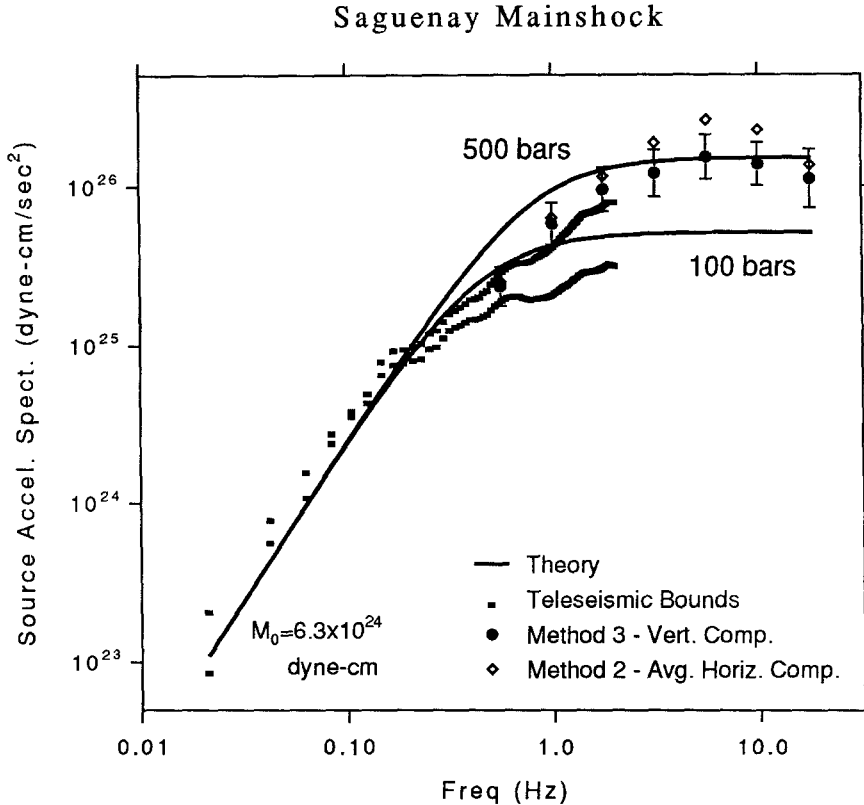


FIG. 19. Source acceleration spectrum of the mainshock estimated from many sources. The teleseismic bounds are from the analysis of  $P$  waves by Boatwright and Choy (1992). The rest of the estimates are from the dominant motion ( $S$  and  $Lg$ ) at distances within 1000 km, using the two methods, discussed in the text, that rely on the synthetic seismograms. Note the difference in ordinate and abscissa scales between Figure 18 and this figure. Theoretical estimates are shown for two stress parameters, 100 and 500 bars, and use the moment determined from long-period data at teleseismic distances. The error bars are estimates of the 68% confidence limits for the source spectrum determined from the estimation method using averages over distance and azimuth before combining the observed and synthetic spectra; the error includes uncertainty in measuring the spectra as well as uncertainty in the regression fits shown in Figure 8. A complete estimate of the uncertainty would include the uncertainty in the velocity model and focal mechanism.

predictions of ground motion (Boore and Atkinson, 1987), and the 500 bars value needed to match the high-frequency spectral level). Clearly, the spectral shape is not well described by an  $\omega^{-2}$  model with a single corner frequency. In spite of this, the simple model can be used to predict high-frequency spectral levels with appropriately chosen parameters, and thus can still be useful in predictions for ground motions at frequencies above the corner frequency.

#### Comparison with Other Intraplate Earthquakes

As we have demonstrated, the spectral excitation produced by the mainshock is very different from that of the two smaller events. In this section, we compare various summary measures of the spectral excitation of the three Saguenay earthquakes with those from other earthquakes in intraplate environments.

The relation between the short-period magnitude ( $m_N$ ) and the seismic moment ( $M_0$ ) for many ENA earthquakes is shown in Figure 20. This is a simple way of showing the relation between short- and long-period spectral

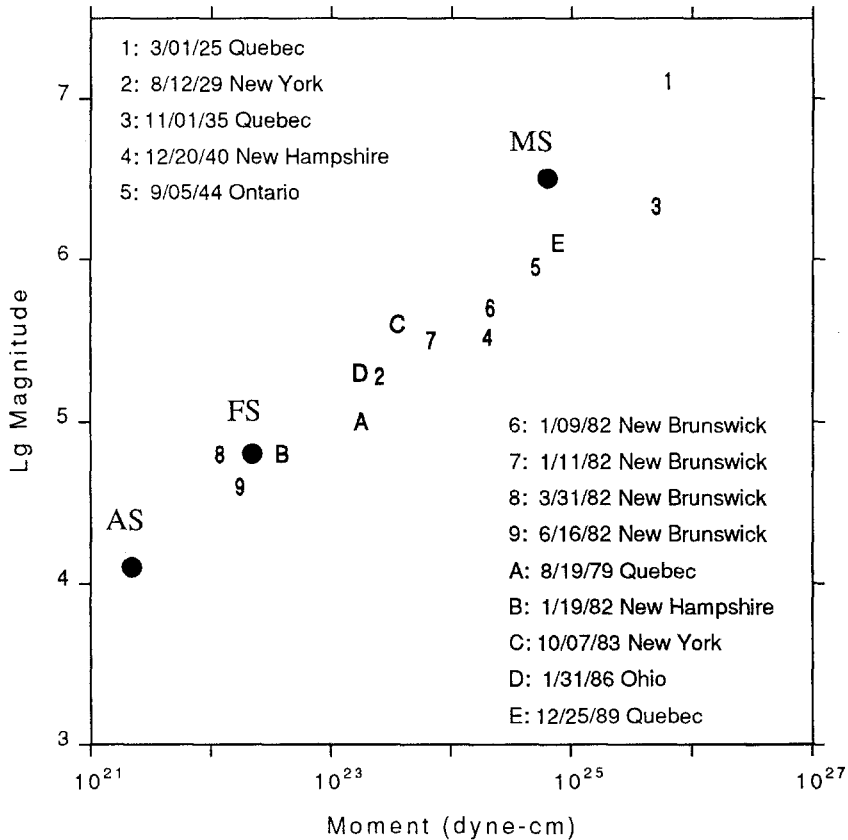


FIG. 20. Short-period (Nuttli) magnitude ( $m_N$ ) versus seismic moment for earthquakes in eastern North America. The Saguenay values are indicated by the large filled circles. The values for the Saguenay earthquakes are from this paper; those for the rest are tabulated in Boore and Atkinson (1987, 1989), using the redeterminations of  $m_N$  in Atkinson and Boore (1987). Multiple estimates of moment have been averaged geometrically. For all the older earthquakes (pre-1950) except for the 1925 Charlevoix event, the moment estimates of Ebel *et al.* (1986) were used in preference to Boore and Atkinson's (1987) revision of the Street and Turcotte (1977) moments; J. Ebel (personal comm., 1991) has indicated that the Ebel *et al.* (1986) moment for the 1925 event is in error.

amplitudes. As others have noted (North *et al.*, 1989), the mainshock is anomalous in that its  $m_N$  is high compared to its  $M_0$ . This observation agrees with the spectral findings from our study. The relation between the short-period magnitude and the seismic moment for the fore- and aftershocks are consistent with other ENA earthquakes. Interestingly, the 1925 Charlevoix earthquake also appears "anomalous." The values of both  $M_0$  and  $m_N$  used for the 1925 event in Figure 20, however, are poorly constrained: the moment estimate is currently under revision by both J. Ebel (personal comm., 1991) and Bent (1992), and the  $m_N$  estimate, which was largely measured at periods much greater than 1 sec (Atkinson and Boore, 1987), may not be indicative of short-period spectral energy.

For many earthquake engineering purposes, the high-frequency source spectral level is of particular concern. The high-frequency spectral levels from the Saguenay earthquakes, estimated from Figure 18, are compared to those from many other intraplate earthquakes in Figure 21. The figure also shows the

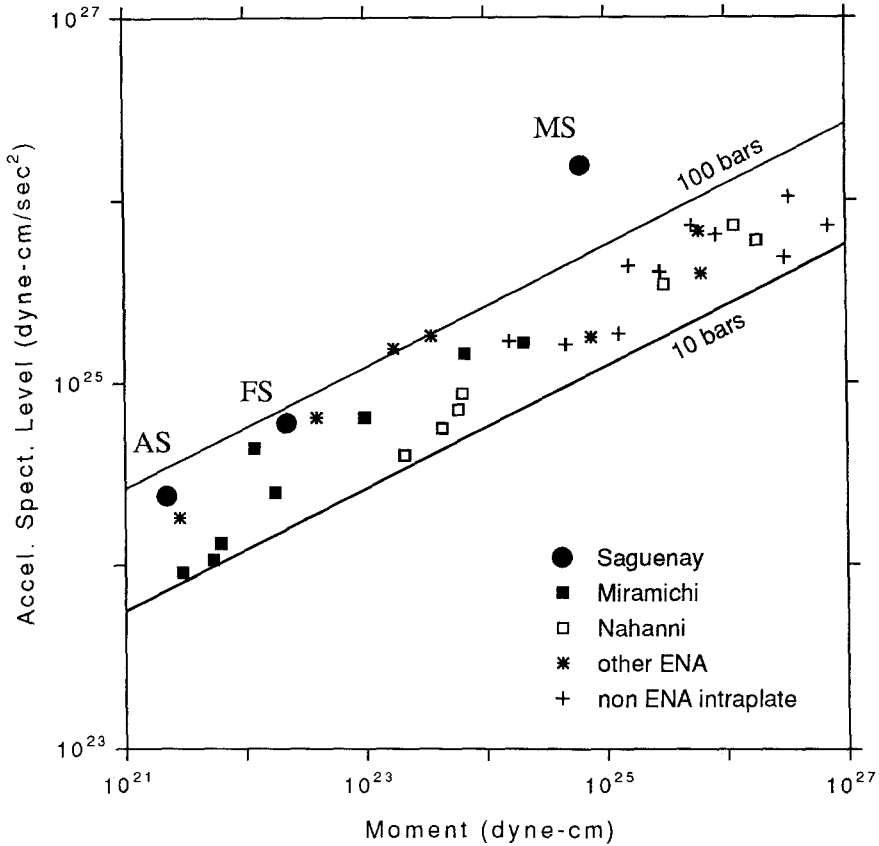


FIG. 21. Observed high-frequency spectral levels for ENA (all symbols except pluses) and other intraplate earthquakes (pluses, from Boatwright and Choy, 1992). The key to the symbols follows: filled circles = 1988 Saguenay, Quebec, foreshock, mainshock, and aftershock; filled squares = 1982 Miramichi, New Brunswick, mainshock and aftershocks; squares = 1985 to 1988 Nahanni, Northwest Territories, mainshocks and aftershocks; asterisks = other ENA mainshocks. Multiple estimates of either spectral level or moment for a particular earthquake have been averaged geometrically. See Table 3 in Boore and Atkinson (1989) for sources of data.

predictions of the  $\omega^{-2}$  model for stress parameters of 10 and 100 bars. The high-frequency level of the Saguenay mainshock is clearly larger than those for other ENA and intraplate events of similar size (including the 1925 Charlevoix earthquake). The foreshock and aftershock are consistent with the other data. Boore and Atkinson (1989) note that the scaling of aftershock sequences (squares in Fig. 21) may be different from that of the corresponding mainshock (stars for ENA and pluses for intraplate earthquakes in other part of the world), with the mainshock having a larger stress parameter than the aftershocks.

#### *Implications for Predicting Ground Motions: Some Comments*

A key question is to what extent the Saguenay mainshock should influence the prediction of future ground motions and earthquake-resistant design. We do not have an answer to this question. The Saguenay mainshock is clearly anomalous relative to other intraplate earthquakes (and, based on our experience, relative to plate margin events as well). On the other hand, the event did occur and, unless physical reasons for the peculiar nature of the event can be

identified that do not exist elsewhere, the event cannot be ignored for design purposes. The relatively normal stress parameters of the fore- and aftershocks suggest that the focal depth (about 28 km for the three events) is not solely responsible for the high stress parameter for the mainshock. On the other hand, studies of aftershocks near Oroville, California (Fletcher *et al.*, 1984) found that the *maximum* stress drop increases with depth; thus stress parameters as large as 500 bars might not be possible for shallower sources.

To improve the prediction of ground motions from future large earthquakes, it may be necessary to consider more complex spectral models than the usual single-corner-frequency model. For example, Atkinson (1990) has suggested that the use of two corner frequencies for larger ENA earthquakes might form the basis of a model with which most of the current data could be reconciled (only one corner would be required for earthquakes smaller than magnitude 5.5). This would be consistent with the theoretical concepts suggested by a number of authors, including Joyner (1984) and Boatwright (1988), and the intraplate data analyses presented by Choy and Boatwright (1988) and Boatwright and Choy (1992). The lower corner might be related to overall fault rupture characteristics and be consistent with a constant-stress parameter of, say 50 bars. The second (higher-frequency) corner, which could be related to the stress required to break the highest-stress asperities on the fault surface, might vary widely from one earthquake to another. Obviously, a key to the success of such a two-corner model for the prediction of motions in future earthquakes is the specification of the higher-frequency corner. This may be difficult unless it is related to physical characteristics of certain local areas or tectonic regimes.

The utility of two-corner-frequency models has been demonstrated in several studies of the Saguenay mainshock. Atkinson (1992) used a general two-corner spectral model, defined by moment magnitude  $M$  and  $m_N$ , to generate stochastic time histories for a Saguenay-type event. This model could be useful in predicting motions for "what if?" studies. Boore (1992) performed similar computations using a two-corner source spectrum fit to Boatwright and Choy's (1992) source spectrum inferred from teleseismic recordings. In both studies, information about the high-frequency radiation was incorporated into the studies (indirectly through the specification of  $m_N$  in Atkinson's case and directly in Boore's study), and as a result the models used in the studies may have little predictive value.

#### CONCLUSIONS

Source spectra were derived from data at distances from about 50 to 700 km, using three different schemes to correct the observed spectra for source excitation and wave propagation effects. Two of the schemes made use of synthetic seismograms, but the results using these methods differ little from those using a simple model in which  $1/R$  geometrical spreading and uniform media are assumed.

The source spectral shape for the mainshock is not well described by an  $\omega^{-2}$  model with a single corner frequency. The spectrum lacks energy at intermediate frequencies (the "Case of the Missing Moment"). For frequencies above about 3 Hz, the source acceleration spectrum is relatively flat, consistent with the  $\omega^{-2}$  model. The implied stress parameter required to match this level is very high (on the order of 500 bars).

The foreshock and the largest aftershock, which occurred at depths similar to

that of the mainshock, have source spectra that are well described by a single-corner-frequency  $\omega^{-2}$  model. Most importantly, a moderate stress parameter of about 65 bars is required to match the high-frequency spectral level. Seismic moments of  $2.2 \times 10^{22}$  and  $2.2 \times 10^{21}$  dyne-cm were estimated for the fore- and aftershocks, respectively.

The spectra at the two closest stations show little evidence of an  $f_{max}$  for frequencies less than about 25 Hz. This was expected for the hard-rock sites in the region. In contrast, a distinct  $f_{max}$  at about 10 Hz is evident at many of the other sites (which differ from the two closest sites both in azimuth and distance). This may be due in part to whole-path attenuation, but the sharpness of the corner suggests that local site effects are also acting to influence the spectral decay.

A frequency-dependent  $Q$  given by  $Q = 755f^{0.52}$  is a good representation of the average anelastic attenuation for data beyond 100 km, assuming a geometrical spreading of  $1/\sqrt{R}$ . We find support for the observations of Hough *et al.* (1989) that the attenuation of motion is not isotropic about the source. Waves propagating along the strike of the St. Lawrence River (which is also the strike of the structural grain) appear to attenuate less rapidly than those propagating perpendicularly to this strike. The boundary between the Grenville and Appalachian tectonic provinces largely coincides with the St. Lawrence River. Whether the different attenuation is due to different anelastic and structural properties in the tectonic provinces or to an anisotropy induced by the structural grain is impossible to determine given the azimuthally nonuniform distribution of data. Accounting for the differences in attenuation makes little difference in the azimuthally averaged source spectra that are the primary goal of this paper.

Estimates of the horizontal-to-vertical spectral ratio from the three-component recordings yielded the relation  $H/V = 1.14 + 0.118f - 0.00638f^2$ . No dependence of this ratio on distance was found.

The high-frequency amplitudes from the Saguenay mainshock are of particular interest, since they exceed median predicted levels (e.g., Boore and Atkinson, 1987; Toro and McGuire, 1987; Atkinson and Boore, 1990) by a significant margin. Based on a comparison of magnitude-moment relations for large eastern earthquakes, and evaluation of high-frequency spectral levels from a suite of intraplate events, we conclude that the high-frequency radiation from the Saguenay mainshock is not typical of large eastern events.

#### ACKNOWLEDGMENTS

We thank the Geological Survey of Canada, and in particular Phil Munro and Bill Shannon, for providing us with the ground-motion data. Paul Friberg provided data from the NCEER-Lamont network in the United States, and J. Drysdale provided the intensity data. Phil Munro and Bob North were very helpful in the interpretation of the instrument-corrected data. We also acknowledge useful discussions with Jack Boatwright, Bill Joyner, and Tom Hanks; Jack and Bill provided constructive and critical reviews of the paper, as did C. B. Crouse and Bob Herrmann. Chuck Mueller's data analysis programs (Mueller, 1990) were invaluable. Special thanks goes to Harley Benz for computing the synthetic seismograms that were used to extract the source spectra from the recorded spectra. This work was partially supported by Ontario Hydro and the U.S. Nuclear Regulatory Commission. We thank these agencies for their continued support of our work.

#### REFERENCES

- Armbruster, J. G. and L. Seeber (1987). Seismicity and seismic zonation along the Appalachians and the Atlantic seaboard from intensity data, in *Proc. Symp. Seismic Hazards, Ground*

- Motions, Soil-Liquefaction, and Engineering Practice in Eastern North America*, K. H. Jacob, Editor, National Center for Earthquake Engineering Research Report NCEER-87-0025, 163-177.
- Atkinson, G. M. (1989). Attenuation of the  $L_g$  phase and site response for the Eastern Canada Telemetred Network, *Seism. Res. Lett.* **60**, 59-69.
- Atkinson, G. M. (1990). A comparison of eastern North America ground motion observations with theoretical predictions, *Seism. Res. Lett.* **61**, 171-180.
- Atkinson, G. M. (1991). Reply to comment by Hough *et al.* (1991), on "A comparison of eastern North America ground motions with theoretical predictions," *Seism. Res. Lett.* **62**, 147-149.
- Atkinson, G. M. (1992). Simple ground motion prediction for the Saguenay earthquake, *Proc. EPRI/USGS/Stanford Workshop on Ground Motion Modeling* (in press).
- Atkinson, G. M. and D. M. Boore (1987). On the  $m_N$ ,  $M$  relation for eastern North America, *Seism. Res. Lett.* **58**, 119-124.
- Atkinson, G. and D. Boore (1990). Recent trends in ground motion and spectral response relations for North America, *Earthquake Spectra* **6**, 15-36.
- Bent, A. L. (1992). A re-examination of the 1925 Charlevoix, Quebec, earthquake, *Bull. Seism. Soc. Am.* **82** (in press).
- Boatwright, J. (1988). The seismic radiation from composite models of faulting, *Bull. Seism. Soc. Am.* **78**, 489-508.
- Boatwright, J. and G. Choy (1992). Acceleration source spectra for large earthquakes in northeastern North America, *Bull. Seism. Soc. Am.* **82**, 660-682.
- Boore, D. M. (1992). Predictions of response spectra for the Saguenay earthquake, *Proc. EPRI/USGS/Stanford Workshop on Ground Motion Modeling* (in press).
- Boore, D. and G. Atkinson (1987). Stochastic prediction of ground motion and spectral response parameters at hard-rock sites in eastern North America, *Bull. Seism. Soc. Am.* **77**, 440-467.
- Boore, D. and G. Atkinson (1989). Spectral scaling of the 1985-1988 Nahanni, Northwest Territories, earthquakes, *Bull. Seism. Soc. Am.* **79**, 1736-1761.
- Bowman, J. R. and B. L. N. Kennett (1991). Propagation of  $L_g$  waves in the North Australian craton: influence of crustal velocity gradients, *Bull. Seism. Soc. Am.* **81**, 592-610.
- Brune, J. (1970). Tectonic stress and the spectra of seismic shear waves from earthquakes, *J. Geophys. Res.* **75**, 4997-5009.
- Campillo, M., M. Bouchon, and B. Massinon (1984). Theoretical study of the excitation, spectral characteristics, and geometrical spreading of regional seismic phases, *Bull. Seism. Soc. Am.* **74**, 79-90.
- Choy, G. and J. Boatwright (1988). Teleseismic and near-field analysis of the Nahanni earthquakes, Northwest Territories, Canada, *Bull. Seism. Soc. Am.* **78**, 1627-1652.
- Cranswick, E. (1988). The information content of high-frequency seismograms and the near-surface geologic structure of "hard rock" recording sites, *Pure Appl. Geophys.* **128**, 333-363.
- Cranswick, E., R. Wetmiller, and J. Boatwright (1985). High-frequency observations and source parameters of microearthquakes recorded at hard-rock sites, *Bull. Seism. Soc. Am.* **75**, 1535-1567.
- Ebel, J. E., P. G. Somerville, and J. D. McIver (1986). A study of the source properties of some large earthquakes of northeastern North America, *J. Geophys. Res.* **91**, 8231-8247.
- Fletcher, J., J. Boatwright, L. Haar, T. Hanks, and A. McGarr (1984). Source parameters for aftershocks of the Oroville, California, earthquake, *Bull. Seism. Soc. Am.* **74**, 1101-1123.
- Friberg, P., R. Busby, D. Lentichia, D. Johnson, K. Jacob, and D. Simpson (1988). The  $M = 6$  Chicoutimi earthquake of Nov. 25, 1988 in the Province of Quebec, Canada: Preliminary NCEER Strong Motion Data Report, Lamont Doherty Geological Observatory, Palisades, New York.
- Gariel, J.-C. and K. H. Jacob (1989). The Saguenay earthquake of November 25, 1988: the effect of the hypocentral depth on the peak acceleration attenuation—a modeling approach, in *The Saguenay Earthquake of November 25, 1988, Quebec, Canada: Strong Motion Data, Ground Failure Observations, and Preliminary Interpretations*, K. H. Jacob, Editor (preliminary version of NCEER report, dated January 89), 83-100.
- Haddon, R. A. W. (1992). Waveform modeling of the strong motion data for the Saguenay earthquake of 25 November 1988, *Bull. Seism. Soc. Am.* **82**, 720-754.
- Hanks, T. C. (1982).  $f_{max}$ , *Bull. Seism. Soc. Am.* **72**, 1867-1879.
- Herrmann, R. and A. Kijko (1983). Modeling some empirical vertical component  $L_g$  relations, *Bull. Seism. Soc. Am.* **73**, 157-171.

- Hough, S. E., K. Jacob, and P. Friberg (1989). The 11/25/88,  $M = 6$  Saguenay earthquake near Chicoutimi, Quebec: evidence for anisotropic wave propagation in northeastern North America, *Geophys. Res. Lett.* **16**, 645–648.
- Joyner, W. (1984). A scaling law for the spectra of large earthquakes, *Bull. Seism. Soc. Am.* **74**, 1167–1188.
- Mueller, C. (1990). *Computer programs for analyzing digital seismic data*, U. S. Geol. Surv. Open-File Rept. 90-35, 100 pp.
- Munro, P. and D. Weichert (1989). *The Saguenay earthquake of Nov. 25, 1988: processed strong motion records*, Geol. Surv. Canada Open-file Rept. 1996.
- North, R., R. Wetmiller, J. Adams, F. Anglin, H. Hasegawa, M. Lamontagne, R. DuBerger, L. Seeber, and J. Armbruster (1989). Preliminary results from the Nov. 25, 1988 Saguenay (Quebec) earthquake, *Seism. Res. Lett.* **60**, 89–93.
- Ou, G.-B. and R. B. Herrmann (1990). A statistical model for ground motion produced by earthquakes at local and regional distances, *Bull. Seism. Soc. Am.* **80**, 1397–1417.
- Shin, T.-C. and R. B. Herrmann (1987).  $Lg$  attenuation and source studies using the 1982 Miramichi data, *Bull. Seism. Soc. Am.* **77**, 384–397.
- Somerville, P. G., J. P. McLaren, C. K. Saikia, and D. V. Helmberger (1990). The 25 November 1988 Saguenay, Quebec earthquake: source parameters and the attenuation of strong ground motion, *Bull. Seism. Soc. Am.* **80**, 1118–1143.
- Street, R. L. and F. T. Turcotte (1977). A study of northeastern North America spectral moments, magnitudes, and intensities, *Bull. Seism. Soc. Am.* **67**, 599–614.
- Street, R. L., R. B. Herrmann, and O. W. Nuttli (1975). Spectral characteristics of the  $Lg$  wave generated by central United States earthquakes, *Geophys. J. R. Astr. Soc.* **41**, 51–63.
- Toro, G. and R. McGuire (1987). An investigation into earthquake ground motion characteristics in eastern North America, *Bull. Seism. Soc. Am.* **77**, 468–489.
- Woodgold, C. (1990). Estimation of  $Q$  in eastern Canada using coda waves, *Bull. Seism. Soc. Am.* **80**, 411–429.
- Zhao, L.-S. and D. V. Helmberger (1992). Broadband modeling along a regional shield path, Harvard recording of the Saguenay earthquake, *Geophys. J.* **105**, 301–312.

#### APPENDIX A: VARIATIONS OF $f_{max}$

A feature in the observed spectra at station S16, as shown in Figure 3, is the apparent lack of a high-frequency corner (commonly known as  $f_{max}$ , after Hanks, 1982) for frequencies as high as 25 Hz. This is in accord with our view (Boore and Atkinson, 1987; Atkinson, 1989) that, unlike rock sites in western North America (with  $f_{max}$  commonly around 5 to 15 Hz), those in eastern North America produce little attenuation at high frequencies. Such a difference has a profound influence on predictions of peak acceleration and high-frequency response spectra at distances small enough that the whole-path anelastic attenuation has not removed the high frequencies from the ground motion. The lack of an  $f_{max}$ , at least on the horizontal components, is shared by the next closest station to the earthquake (S17), as shown in Figure A1. A striking feature of Figure A1, however, is that the spectra from almost all the other stations have an  $f_{max}$ , usually at frequencies near 10 Hz. As far as we know, there is nothing unusual about the site conditions of S16 and S17 relative to the other sites; they are all hard-rock, glaciated sites. S16 and S17, however, are closer to the earthquake and are at distinctly different azimuths than the other stations (Fig. 1). This might mean that the difference in the high-frequency behavior is a source or propagation effect rather than a local site effect. Source directivity can produce shifts in the corner frequency defined by the change from a rising acceleration spectrum at low frequencies to the level portion at higher frequencies; to our knowledge, however, shifts in the higher-frequency  $f_{max}$  are not explained by source theory. If a source property is the origin of  $f_{max}$ , however (a view that is actively debated), then the azimuthal dependence could well be a source property.

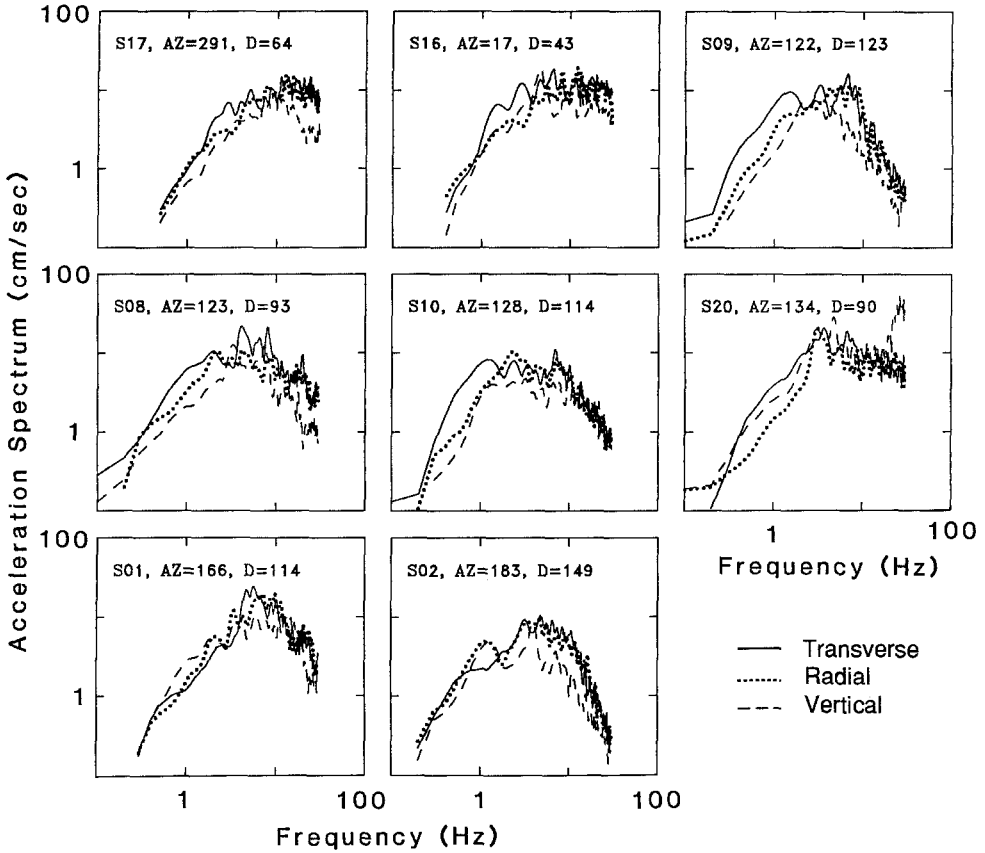


FIG. A1. Fourier acceleration spectra (not corrected back to the source) for all SMA rock sites, arranged by source-to-station azimuth (AZ, in degrees clockwise from north; the epicentral distance in km is given by D). The window length for computing the spectra was generally 15 or 20 sec, with an 11 sec window used for S20.

To emphasize the difference in the spectra, we show in Figure A2 a direct comparison between the spectra at S16 and S10. Also shown are the acceleration time series. In addition to the obvious difference in  $f_{max}$ , this figure also points out another interesting feature in the records: the unusually complicated time series at S16 relative to that at S10 (the time series at S17 shares this feature, and S10 is not alone in having a relative short-duration time series). Synthetic seismograms (e.g., Fig. 11 in Somerville *et al.*, 1990) predict that stations S16 and S17 should have a short duration of large motion, in distinct disagreement with the observations.

As a first step in investigating the possibility that a path effect is responsible for the differences in  $f_{max}$ , we show in Figure A3 that a simple model with a constant  $Q$  of about 1000 acting over the entire travel path produces the observed spectral decay for the more distant station but predicts too much attenuation for the closer station. On the other hand, the frequency-dependent  $Q$  found in our analysis of the  $Lg$  data does not produce enough attenuation at the more distant station. Cranswick *et al.* (1985; see also Cranswick, 1988) argue that although whole-path attenuation can model the overall spectral decay, such attenuation produces smooth changes in the spectrum. They further

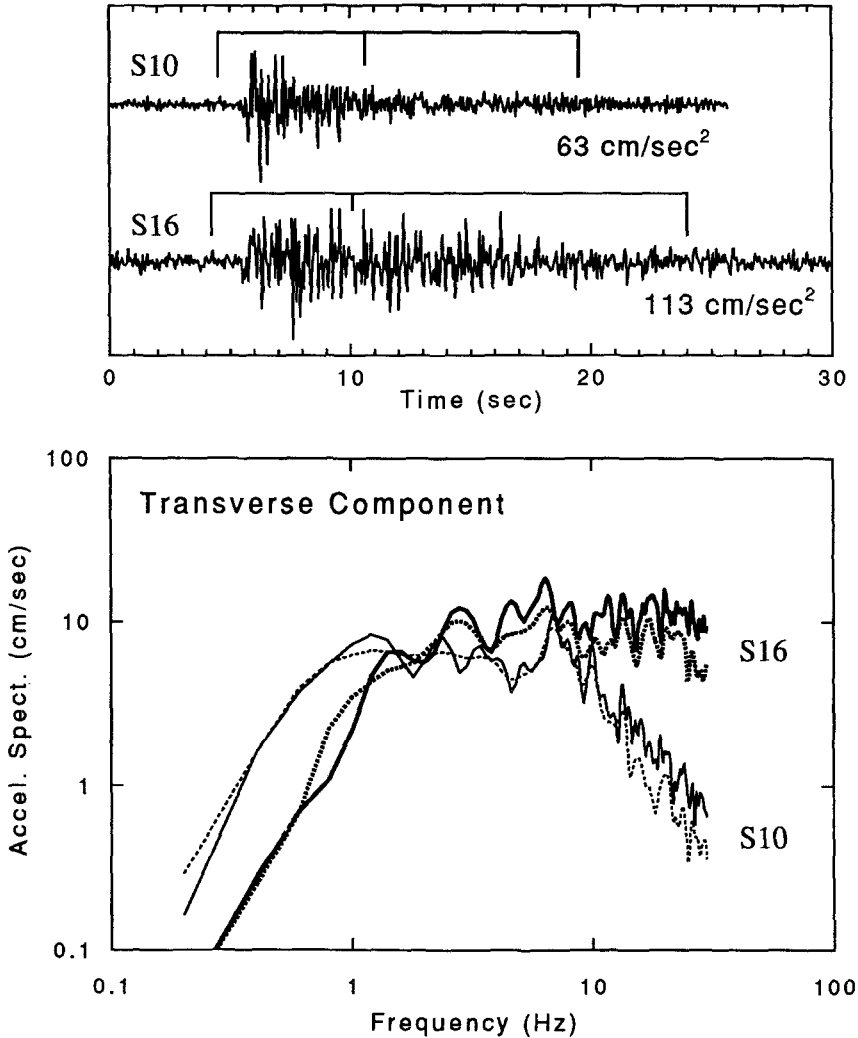


FIG. A2. Time series and Fourier acceleration spectra for the transverse component at S10 and S16. Notice the pronounced difference in the high-frequency attenuation of the spectra, even though both sites are on apparently competent rock. The time series for the two traces are shown above (labeled with peak amplitudes on the right). To show the effect of window length, spectra were computed using a short window of 6 sec (dots) and long windows of 15 and 20 sec for stations S10 and S16, respectively.

argue that sharp changes, such as seen at S10, might indicate that the spectral decay is associated with local site resonances (the peak in the S10 spectrum at 7 Hz might be due such a resonance). The data necessary to assess the relative contribution of source, path, and site effects to the observed  $f_{max}$  have yet to be collected.

#### APPENDIX B: THEORETICAL SOURCE SPECTRUM

Although published in many other places, for convenience we repeat here the equations for the source acceleration spectra corresponding to the constant stress parameter, single-corner-frequency model. The source acceleration

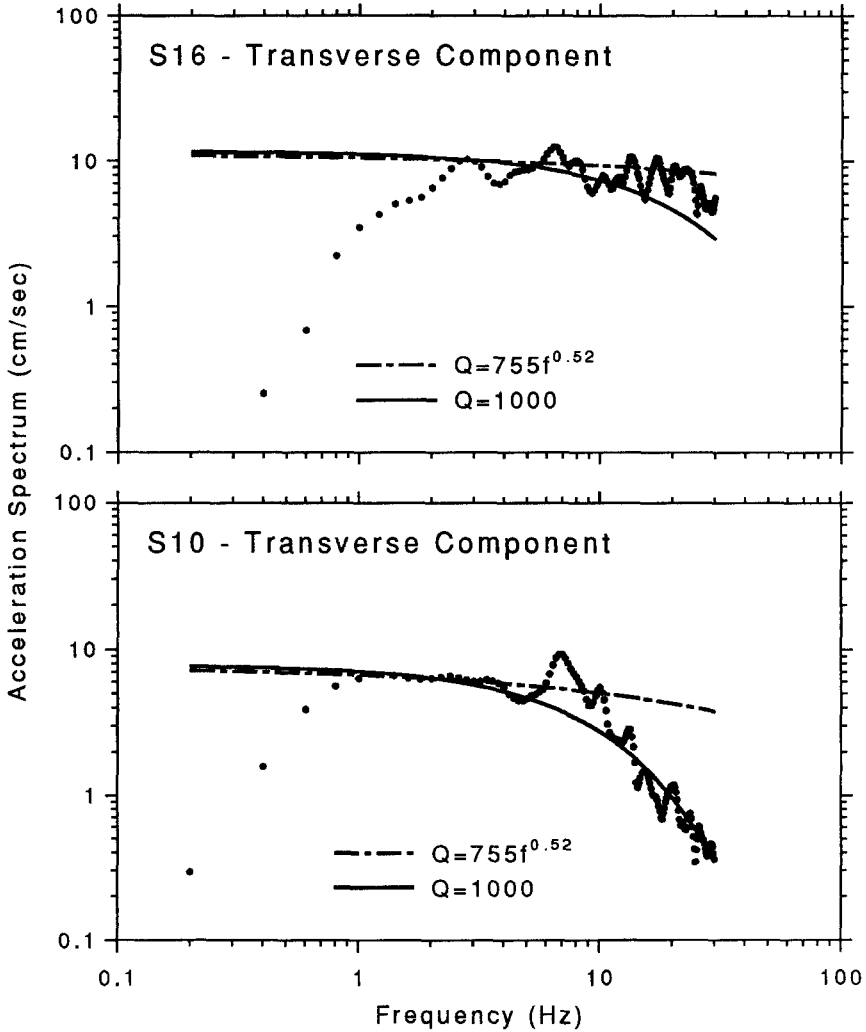


FIG. A3. The spectra for the transverse component of motion at S10 and S16 (computed for the short time window shown in Figure A2), compared with whole-path attenuation using  $Q = 1000$  and  $Q = 755f^{0.52}$ . The observed spectra are shown by filled circles, and the theoretical spectra are shown by lines; the curves have been adjusted vertically to approximately match the observed spectra at 3 Hz. The frequency-dependent equation for  $Q$  was obtained by fitting the attenuation of the  $Lg$  waves (although the motions at S10 and S16 are not  $Lg$  waves, the  $Lg$  attenuation should be a good approximation to the overall attenuation in the crust).

spectrum  $S_a(f)$  is

$$S_a(f) = \omega^2 S(f), \quad (\text{B1})$$

where  $\omega = 2\pi f$  and the moment-rate function  $S(f)$  approaches the seismic moment  $M_0$  for low frequencies. For the Brune (1970)  $\omega^{-2}$  model,  $S(f)$  is given by

$$S(f) = M_0 / [1 + (f/f_0)^2]. \quad (\text{B2})$$

The source corner frequency  $f_0$  is related to the seismic moment ( $M_0$ ) and the stress parameter ( $\Delta\sigma$ ) by

$$f_0 = 4.9 \times 10^6 \beta_0 (\Delta\sigma / M_0)^{1/3}, \quad (\text{B3})$$

where the shear velocity near the source ( $\beta_0$ ) has units of km/sec, and the units of  $M_0$  and  $\Delta\sigma$  are dyne-cm and bars, respectively.

U. S. GEOLOGICAL SURVEY  
MAIL STOP 977  
345 MIDDLEFIELD ROAD  
MENLO PARK, CALIFORNIA 94025  
(D.M.B.)

125 DUNBAR ROAD SOUTH  
WATERLOO, ONTARIO N2L 2E8  
CANADA  
(G.M.A.)

Manuscript received 17 May 1991